Preclinical Study of Cannflavins A and B Action Against Glioblastoma Cells

Jennifer Holborn [a], Hannah Robeson [a,1], Ellis Chartley [a,1], Tiana Gluscevic [a,b,1], Adina Borenstein [a], Colby Perrin [a], Begüm Alural [a], Himain Perera [a], Tariq A. Akhtar [a], Nina Jones [a], Jasmin Lalonde [a,*]

[a] Department of Molecular and Cellular Biology, University of Guelph, 50 Stone Road E, Guelph, ON N1G 2W1, Canada

[b] Canurta Therapeutics, 2425 Matheson Blvd. E, Suite 807, Mississauga, ON, L4W 5K4, Canada

[1] These authors contributed equally to this study.

* Corresponding author: **Jasmin Lalonde**

Email address: jlalon07@uoguelph.ca

Phone: (519) 824-4120 x. 54706

ORCID: 0000-0002-6797-1894 (J. Lalonde)

Keywords: Cannflavins, Cerebral organoids, Flavonoids, Glioblastoma multiform, Invasion, Migration

22 *Abbreviations:* AKT, Protein kinase B; BDNF, Brain-Derived Neurotrophic Factor; BSA,
23 Bovine Serum Albumin; DMEM, Dulbecco's Modified Eagle's Medium; DMSO,
24 Dimethylsulfoxide; FBS, Fetal Bovine Serum; GBM, Glioblastoma multiform; GFP,
25 Green Fluorescent Protein; iPSC, induced Pluripotent Stem Cell; MAPK, Mitogen-
26 Activated Protein Kinase; mTOR, mammalian target of rapamycin; NF-κB, Nuclear factor-
27 κB; PBS, Phosphate Buffered Saline; RTK, Receptor Tyrosine Kinase; TMZ,
28 Temozolomide; TrkB, Tropomyosin receptor kinase B.

ABSTRACT

Background: Flavonoids represent a large group of naturally occurring polyphenolic compounds, many of which have been found to produce valuable biological outcomes, including action against cancer cells. Glioblastoma multiforme (GBM) is an aggressive type of brain tumor that is associated with a poor prognosis and has limited treatment options. Previous findings suggest that cannflavins can produce promising effects for pancreatic and bladder cancers, but the efficacy of these phytochemicals in attacking brain tumour cells remains unknown. Our study evaluates the potential of cannflavin A and cannflavin B against GBM cells using a range of *in vitro* approaches.

Results: We conducted experiments using A-172 and U-87 GBM lines to assess the impact of cannflavins A and B on cell viability, cycle, migration, and invasion capacity. Our results revealed a consistent dose-dependent decrease in cell viability in both lines after the addition of cannflavin B to the culture media. Interestingly, we found that chrysoeriol (the non-prenylated synthesis precursor of cannflavins in the *Cannabis sativa* plant) only has a limited adverse effect on survival using the same approach, while techtochrysin (an O-methylated flavone) has none. Using time-lapse live-cell imaging and a scratch assay, we also show that cannflavins can inhibit tumor cell migration at concentrations below those that produce significant cell death. Finally, we found that cannflavin B exhibits anti-migratory and anti-invasive properties in transwell and tumorsphere assays, underscoring its multifaceted therapeutic potential.

Conclusion: These findings suggest that cannflavin B holds promise as a therapeutic agent in the treatment of GBM.

51 **HIGHLIGHTS (3-5 BULLET POINTS)**

52 • Cannflavin B but not cannflavin A limits the viability of A-172 and U-87 GBM cells
53 in a concentration- and time-dependent manner.
54 • Using time-lapse live-cell imaging and a scratch assay, we provide evidence that
55 cannflavins A and B can inhibit GBM cell migration at concentrations below those
56 that result in a significant reduction in cell viability.
57 • Cannflavin B exhibits robust anti-migratory and anti-invasive properties in transwell
58 and tumorsphere assays, underscoring its multifaceted therapeutic potential.
59 • Although previous work had reported the capacity of cannflavins A and B to interfere
60 with TrkB and downstream the MAPK/AKT signaling pathways in mouse primary
61 neurons, the effect of those molecules is limited in GBMs, suggesting that other targets
62 are engaged to produce the cellular effects.
63

64 **INTRODUCTION**

65 Flavonoids are naturally occurring polyphenolic molecules that accumulate in dietary items
66 such as fruits, vegetables, and teas. This broad group of phytochemicals has received
67 considerable research attention for over 25 years due to their beneficial anti-inflammatory
68 and anti-oxidative properties (Panche *et al.*, 2016). Many flavonoids have also attracted
69 interest in cancer research due to their potential therapeutic applications. For instance,
70 kaempferol has been found to induce G2/M cell cycle arrest as well as reduce migration
71 and invasion in breast, liver, ovarian, lung, and brain cancers (Gao et al., 2018; Jo et al.,
72 2015; Li et al., 2017; Zhu et al., 2019). Apigenin and luteolin, for their part, have shown
73 promise as anti-cancer agents for breast, prostate, lung, and brain subtypes by suppressing
74 the mitogen-activated protein kinase (MAPK) and Protein kinase B (AKT) signaling
75 pathways that control cell proliferation and survival (Cheng et al., 2013; Erdogan et al.,
76 2016; Huang et al., 2019; Tseng et al., 2017). Finally, quercetin, one of the most consumed
77 dietary flavonoids, induces G2/M phase arrest and significantly increases tumor suppressor
78 protein p53 expression in MDA-MB-453 breast cancer cells (Choi et al., 2008). It also
79 limits angiogenesis and metastasis of other cancer cell types through changes in
80 MAPK/AKT/mTOR signaling pathways (Balakrishnan et al., 2016; Gao et al., 2012; Kim
81 et al., 2019; Lee et al., 2015; Pratheeshkumar et al., 2012). Taken together, these examples
82 support searching for additional flavonoids that also produce robust anti-cancer effects.

83 Cannflavins are prenylated and highly lipophilic metabolites first purified 40 years ago
84 from *Cannabis sativa (C. sativa)* plant extracts (Barrett et al., 1985). As illustrated in
85 **Supplementary Figure 1**, the cannflavin family includes five known members, which are
86 cannflavin A, cannflavin B, cannflavin C, isocannflavin B (also known as FBL-03G), and

87 8-prenylcannflavin B (also known as dorsmanin D). Several of these molecules have been
88 shown to produce promising effects applicable to various clinical conditions. For instance,
89 studies revealed the anti-inflammatory properties of cannflavins A and B through their
90 ability to inhibit pro-inflammatory mediators and the production of prostaglandin E_2 at a
91 rate thirty times more potent than aspirin (Barrett et al., 1985; Werz et al., 2014). Consistent
92 with their anti-inflammatory activity, Eggers and colleagues (2019) have reported
93 neuroprotective action of cannflavin A in neuronal PC12 cells against amyloid β-induced
94 cell death by reducing $A\beta_1$-42 aggregation and fibril formation.

95 Beyond studies concerning inflammation, other research suggests that specific
96 cannflavin molecules exhibit desirable anti-cancer effects that may involve other pathways.
97 For instance, isocannflavin B was found to improve survival in preclinical mouse models
98 of metastatic pancreatic cancer by increasing apoptosis of tumor cells (Moreau et al., 2019),
99 and cannflavin A has been reported to synergize with agents commonly used to treat
100 bladder cancer at specific concentrations (Tomko et al., 2022). Despite those promising
101 results, whether cannflavins can effectively attack brain cancer cells has not been directly
102 studied.

103 Glioblastoma multiforme (GBM) is the most aggressive and common primary brain
104 tumor in adults, characterized by rapid growth and diffuse infiltration into surrounding
105 healthy brain tissues (Tilak et al., 2021a). The prognosis for GBM patients is extremely
106 poor, with a median survival of approximately 15 months despite aggressive treatment
107 (Johnson and O'Neill, 2012; Ostrom et al., 2020). The standard of care for GBM is
108 maximum safe surgical resection followed by a combination of radiation therapy and
109 temozolomide (TMZ) chemotherapy, a DNA alkylating agent that induces cell death

110 through DNA lesions (Stupp et al., 2005; Stupp et al., 2009; Fisher and Adamson, 2021).
111 However, the inability to fully resect the tumor with surgery, combined with the persistence
112 of TMZ-resistant cancer cells capable of recapitulating tumors, typically leads to disease
113 relapse within just a few months (Weller et al., 2013; Birzu et al., 2020). Therefore, there
114 is a pressing need to identify new agents that could improve patient prognosis.

115 In this study, we conducted experiments using the A-172 and U-87 GBM cell lines to
116 assess the effects of cannflavins A and B on cell viability, migration, and invasion. Our
117 work revealed a decrease in GBM cell viability with increasing concentrations of
118 cannflavin B. Additionally, analysis of cell migration using a time-lapse live-cell scratch
119 assay revealed the potential of cannflavins to impede tumor dissemination at concentrations
120 below those inducing cell death. Specifically, cannflavin B exhibited robust anti-migratory
121 and anti-invasive properties, as evidenced by transwell and tumorsphere invasion assays,
122 highlighting its multifaceted therapeutic effects. Finally, as our previous work found
123 interference of TrkB signaling by cannflavin A and cannflavin B in mouse primary neurons
124 (Holborn et al., 2023), we also evaluated whether the action of cannflavins on GBM cells
125 could be tied to reduced activity of this receptor tyrosine kinase (RTK). Together, our
126 findings underscore the promising anti-cancer properties of cannflavin B against
127 immortalized GBM cells, suggesting its potential role as a novel therapeutic agent.

128 **MATERIALS AND METHODS**

129 *Cell culture and reagents*

130 Malignant male glioma cell lines A-172 and U-87 MG (U-87) were obtained from the
131 American Type Culture Collection (ATCC, USA, Cat No. CRL-1620 and HTB-14,
132 respectively). Cells were cultured in DMEM (Gibco, USA, Cat No. 11965-092)
133 supplemented with 10% FBS (Gibco, Cat No. 12483-020) and 0.5%
134 penicillin/streptomycin (Gibco, Cat No. 155140-122), at 37°C and 5% CO_2. For treatment
135 with cannflavins and other tested agents, the molecules were dissolved in DMSO and
136 applied directly to the culture media.

137 The BIONi010-A cell line (European Bank for induced Pluripotent Stem Cells,
138 ECACC Cat No. 66540022) used to prepare cerebral organoids was purchased from Sigma-
139 Aldrich (St-Louis, MO, USA) and cultured in ExCellerate iPSC Expansion Medium (R&D
140 Systems, Cat No. CCM036) according to the manufacturer's instructions.

141

142 *Antibodies and pharmacological compounds*

143 The antibodies recognizing phosphorylated p44/p42 MAPK (Cat No. 4370), AKT (Cat No.
144 4691), phosphorylated AKT Thr 308 (AKT T308, Cat No. 2965), and phosphorylated AKT
145 Ser 473 (AKT S473, Cat No. 4060) were acquired from Cell Signaling Technology
146 (Beverly, MA, USA). The antibody detecting phosphorylated TrkB Tyr705 (TrkB Y705,
147 Cat No. ab229908) was from Abcam (Waltham, MA, USA), the antibody recognizing p42
148 MAPK (Erk2, sc-1647) was from Santa Cruz Biotechnology (Santa Cruz, CA), the
149 GAPDH (Cat No. AB2302) antibody was from Sigma-Aldrich, and the Tubulin β 3 (TUJ1,
150 Cat No. 801202) antibody was from BioLegend (San Diego, CA, USA). Finally, the GFP

151 (Cat No. 10262) and cross-absorbed secondary antibodies (horseradish peroxidase- and
152 fluorophore-conjugated) were from Invitrogen.

153 Cannflavin A (Cat No. C-291001) and cannflavin B (Cat No. C-291003) were
154 purchased from TLC Pharmaceutical Standards (Newmarket, ON, Canada). ANA-12 (Cat
155 No. SML0209) was acquired from Sigma-Aldrich, and chrysoeriol (Cat No. 491-71-4)
156 from Cayman Chemical (Ann Arbor, MI, USA).

157 Techtochrysin was biosynthesized as follows: The *O. basilicum* O-methyl transferase
158 ObFOMT1 (Accession number JQ653275) open reading frame was synthesized by Twist
159 Bioscience (San Francisco, CA, USA) in the *pET28a* vector system between the *NdeL* and
160 *XhoI* sites. This system inserted an N-terminal hexahistidine tag into the coding sequence.
161 The construct was then introduced into *E. coli* BL21-CodonPlus (DE3)-RIPL. Bacterial
162 cells harboring the expression vector were cultured in LB media at 37°C to an OD_{600} of
163 0.6. Isopropyl-β-D-thiogalactoside was added to a final concentration of 0.2 mM, and
164 cultures were further incubated at 16°C for an additional 16 hours to allow for protein
165 expression. Thereafter, *E. coli* cells were collected by centrifugation, resuspended in Buffer
166 A (20 mM Tris-HCl, 500 mM KCl, pH 8.0) and lysed using an Emulsiflex. Cell debris and
167 remaining intact cells were removed from the solution by centrifugation (20,000 x *g*, 20
168 minutes at 4°C) and the supernatant was applied to a 1 mL HisTrap FF column (Cytiva,
169 Marlborough, MA) equilibrated in Buffer B (20 mM Tris-HCl, 500 mM KCl, 20 mM
170 imidazole, pH 8.0). Proteins bound to the Ni^{2+} affinity matrix were washed with fifteen
171 column volumes of Buffer B, eluted with one column volume of Buffer C (20 mM Tris-
172 HCl, 500 mM KCl, 200 mM imidazole, pH 8.0), and then immediately desalted on PD-10
173 columns (Cytiva) equilibrated with Buffer D (50 mM Tris-HCl, 5 mM $MgCl_2$, pH 8.0, 10%

174 glycerol). The concentration of recombinant ObFOMT1 was determined by Bradford
175 Assay using BSA as a standard, and 1 mg was used per enzymatic assay to produce
176 techtochrysin. Precisely, purified recombinant ObFOMT1 was mixed in 10 mL of assay
177 solution (1 mM chrysin, 10% w/v hydroxypropyl-β-cyclodextrin, 2 mM S-
178 adenosylmethionine, and 5 mM $MgCl_2$ in 50 mM Tris-HCl, pH 8.0) and incubated with
179 shaking for 16 hours at 15°C. Reagents for the assay solution were obtained from Xi'an B-
180 Thriving I/E Co., Ltd (Xi'an, Shaanxi, China). The enzymatic reaction was terminated by
181 adding 1 mL of 10% formic acid. Prenylated bibenzyl products were extracted with three
182 volumes of ethyl acetate three times, evaporated to dryness with gaseous N, and
183 resuspended in 6 mL of methanol. The sample was chromatographed on an Infinity Lab
184 Poroshell 120 EC-C18 2.7 µM (ODS2 9.4 x 150 mm) column and resolved by an Agilent
185 1260 infinity HPLC using a linear gradient with solvent A (45% methanol, 0.1% formic
186 acid in water) and solvent B (95% methanol, 0.1% formic acid in water) at a flow rate of
187 2.5 mL/min heated at 30°C. The gradient started at 60% of solvent B and increased to 70%
188 in 7 minutes, then increased to 100% of solvent B in 1 minute and remained isocratic for 2
189 minutes. Techtochrysin was detected by absorption at 340 nm and was collected from the
190 HPLC at 9.3 minutes. Finally, the eluate was dried under gaseous nitrogen, lyophilized,
191 and techtochrysin quantified relative to a standard curve generated with chrysin. Product
192 identity was confirmed based on mass spectral fragmentation patterns.
193
194 *Cell viability assay*
195 Cell viability was assessed using a resazurin reduction assay, as described previously
196 (Holborn et al., 2023). Briefly, A-172 and U-87 cells were seeded in 96 multi-well plates

197 at a density of 1.0 x 10^4 per well and allowed to attach overnight. Cells were then treated
198 with DMSO and varying concentrations of ANA-12 (1 to 50 μM) or cannflavins (1 to 20
199 μM) diluted in Opti-MEM reduced serum media (Gibco, Cat No. 31985070) and incubated
200 at 37°C for the indicated time. Following treatment, resazurin sodium salt (Sigma-Aldrich,
201 Cat No. R7017) was dissolved in Hank's balanced salt solution (Wisent Inc., Saint-Jean-
202 Baptiste, QC, Canada, Cat No. 311-513-CL), diluted 1:10 in each well, and cells were
203 further incubated at 37°C for three hours. Fluorescence was measured on a microplate
204 reader at 570/590 nm, and a background control was subtracted from each value. All
205 treatments were completed in triplicate.

206 The following procedure was used for quantification: First, fluorescence values were
207 exported from the microplate reader, and the average of three background control wells
208 with Opti-MEM reduced serum media only was subtracted from each treatment value.
209 Second, the subtracted values were multiplied by 100 and divided by the average of the
210 DMSO controls to obtain a percentage relative to the vehicle control. Finally, the average
211 of three replicates per treatment was used as the final value for one biological replicate. A
212 minimum of three biological replicates were taken.

213

214 *Lactate dehydrogenase cytotoxicity assay*

215 Lactate dehydrogenase (LDH) release was measured using the CyQUANT LDH
216 Cytotoxicity Assay Kit according to the manufacturer's protocol (Invitrogen, Cat No.
217 C20300). Briefly, A-172 and U-87 cells were seeded in 96-well multiplates and treated
218 with the tested molecules, using a similar approach to the resazurin reduction assay. Before
219 the treatment endpoint, 10× Lysis Buffer was applied to control wells for 10 minutes to get

220 the Maximum LDH Release value. Cell culture supernatant from each treatment was
221 transferred to a new 96-well multiplate, an equal volume of reaction mixture was added,
222 mixed, and then the plate was incubated at room temperature for 30 minutes, protected
223 from light. Absorbance was measured on a microplate reader at 490 nm and 680 nm
224 (background). All treatments were completed in triplicate.

225 The following procedure was used for quantification: First, LDH activity was
226 calculated by subtracting the raw absorbance value measured at 680 nm from the 490 nm
227 value for each replicate and treatment. The average of three background control wells with
228 Opti-MEM reduced serum media was subtracted from each treatment value. Finally, the
229 LDH activity of each technical replicate of the compound-treated wells was divided by the
230 average of the maximum LDH activity and multiplied by 100 to obtain the percent
231 cytotoxicity. The average of the triplicates per treatment was taken and used as the final
232 value for one biological replicate; three biological replicates were completed in total.

233

234 *Terminal deoxynucleotidyl transferase dUTP nick end labeling (TUNEL) assay*

235 The Roche *in Situ* Cell Death Detection Kit, Fluorescein (Sigma-Aldrich, Cat No.
236 11684795910), was used according to the manufacturer's protocol. Briefly, A-172 cells
237 were fixed using 4% paraformaldehyde for 15 minutes after treatment, then incubated for
238 2 minutes in permeabilization solution (0.1% Triton X-100, 0.1% sodium citrate in PBS).
239 This was followed by a 1-hour incubation in the dark at 37°C with humidity in TUNEL
240 reaction solution. After rinsing with PBS three times for 10 minutes, cells were incubated
241 in 4',6-diamidino-2-phenylindole (DAPI; Invitrogen, Cat No. 62247) staining solution for

242 10 minutes and finally washed in PBS twice for 10 minutes before being mounted onto
243 slides with ProLong Diamond Antifade (Invitrogen, Cat No. P36930).
244
245 *Flow cytometry*
246 A-172 cells and U-87 cells were seeded in 6-well plates at a density of 2.5 x 10^5 per well
247 and allowed to attach overnight. The next day, cells were treated with DMSO control,
248 cannflavin A, or cannflavin B (1 and 5 μM) for 24 hours. Following that time, the cell
249 monolayer was dissociated with trypsin, pelleted, resuspended in FACS buffer (PBS
250 supplemented with 2% FBS and 1 mM EDTA), and frozen fixed at -20°C in 70% ethanol.
251 Immediately before running samples, fixed cells were thawed and washed twice in FACS
252 buffer, 50 μL of 100 μg/mL RNAse A (Thermo Fisher Scientific, Cat No. EN0531) in
253 FACS buffer was added for 30 minutes, then 200 μL of 0.25 μg/mL propidium iodide
254 (Molecular Probes, Cat No. P-1304) in FACS buffer was added for 10 minutes in the dark.
255 The DNA contents were analyzed using a Northern Lights cytometer (Cytek Biosciences,
256 Bethesda, MD, USA).
257 Data quantification was performed using FlowJo v10.10 software. First, debris was
258 excluded using SSC-A vs. FSC-A gating strategy, and then singlets were selected using
259 FSC-H vs. FSC-A. Specifically, the univariate cell cycle platform Watson Pragmatic
260 algorithm distributed cell cycle peaks to the histograms presented, and data points were
261 plotted as a percentage of the cell count found in each cell cycle phase (G1, S, G2/M).

262 *Transwell invasion assay*

263 The bottoms of Corning Transwell inserts (New York, USA, Cat No. CLS3442) were
264 coated with 20 µg/mL fibronectin (Sigma-Aldrich, Cat No. F1141-1MG) at 4°C for 1 hour.
265 After three washes with PBS, the tops were coated with 0.2 mg/mL Corning Matrigel
266 matrix (Cat No. 354234) overnight at 37°C. In parallel with the preparation of the
267 transwells, A-172 cells were seeded at a density of 1.5 x 10^5 cells per well in 6-well plates
268 and grown to 85-90% confluency for 24 hours. They were then treated overnight with 10
269 µM cannflavin B or DMSO in DMEM containing 1% FBS media. The next day, 30,000
270 live cells from each condition were collected and seeded in the upper chamber of each well
271 with DMEM containing 1% FBS plus cannflavin B (10 µM), and in the bottom chamber
272 with DMEM containing 10% FBS. Cells were allowed to invade the Matrigel matrix for
273 24 hours at 37°C and 5% CO_2. Afterward, the transwell membranes containing the invaded
274 cells were removed. The membranes were stained with a 1% crystal violet solution in 20%
275 methanol for 20 minutes, washed three times with PBS, and dried for several hours at room
276 temperature. Representative photographic images of the membranes were taken and then
277 cut out. Finally, crystal violet was eluted from each membrane with 10% acetic acid for 20
278 minutes, and the absorbance (at 562 nm) of the eluates was measured to quantify invasion.
279 Three biological replicates with each treatment run in duplicate were analyzed.

280

281 *Scratch migration assay*

282 A-172 cells were seeded in a 6-well plate at a density of 2.0 x 10^5 per well and grown to
283 complete confluency in DMEM supplemented with 10% FBS for 48 hours. Using a P1000
284 pipette tip, 4 crossing linear wounds were created through the monolayer of cells within

285 each well. Next, the unattached cells were washed away with PBS twice before being added
286 back to 1% FBS DMEM supplemented with DMSO only or the treatment molecules.
287 Baseline images of the wound area were acquired immediately after adding the culture
288 media using a phase-contrast inverted Nikon Eclipse Ti2-E microscope (Nikon
289 Instruments, Melville, NY, USA) equipped with a motorized stage and STXF stage top
290 incubator (Tokai Hit USA Inc., PA, USA) to maintain temperature (37°C), humidity, and
291 CO_2 (5%, 150 mL/min) constant. Two separate areas per scratch were imaged every 15
292 minutes over a 48-hour period. NIS-Elements Advanced Research software was used to
293 run binary area fraction analysis, and the number of migrated cells was counted using
294 ImageJ v1.54 software. Three biological replicates were performed for each treatment
295 condition.
296
297 *Generation of tumorspheres (tumor spheroids)*
298 The tumorsphere protocol was adapted from previous work (Vinci et al., 2015; Tilak et al.,
299 2021b). Briefly, U-87 cells were passaged at least three times in complete media and then
300 20,000 cells per well were seeded into a clear round-bottom ultra-low attachment
301 microplate (Corning, Cat No. 7007). Tumorspheres were allowed to form for 5 days at
302 37°C and 5% CO_2, with half the media changed on Day 3.
303
304 *Tumorsphere invasion assay*
305 Individual tumorspheres prepared as mentioned above were embedded in Corning Matrigel
306 matrix (Cat No. 354234) containing the specified treatment. Four tumorspheres with a
307 circular shape and no protrusions were chosen per treatment, and half the media was

308 removed from the well. An equal volume of Matrigel supplemented with treatment at 2x
309 concentration was added to each well and incubated at 37°C and 5% CO_2 for one hour to
310 polymerize. Treatments at 1x of the desired treatment concentration were prepared in
311 complete media and added to each well immediately after incubation. The plate was then
312 imaged on a Nikon Eclipse Ti2-E inverted microscope equipped with a motorized stage,
313 image stitching capability, and a 10× objective at 0, 24, 48, and 72 hours. One image per
314 tumorsphere per treatment (4 tumorspheres and 4 treatments for 16 images at each time
315 point) was analyzed, and three biological replicates were performed.

316 The image analysis on original tiff files was performed with ImageJ as follows: For
317 the area measurement, the elliptical tool was used to encircle each tumorsphere, ensuring
318 all cells grown out from the original tumorsphere were included in the area measurement.
319 Three area measurements were taken for each tumorsphere at each time point and averaged.
320 For the radius measurement, the line tool was used to measure from the center point of the
321 tumorsphere out to the furthest protrusion from the tumorsphere. Three radius
322 measurements were taken for each tumorsphere at each time point and averaged. The
323 average area or radius of each treatment was divided by the DMSO control average at its
324 corresponding time point to obtain the values used for statistical analysis.

325

326 *Generation of cerebral organoids*

327 BIONi010-A induced pluripotent stem cells (iPSCs) were cultured on Matrigel-coated
328 plates (Corning, Cat No. 354277) in ExCellerate iPSC Expansion Medium (R&D Systems,
329 Cat No. CCM036). Cerebral organoids were generated using the STEMdiff Cerebral
330 Organoid Kit (StemCell Technologies, Cat No. 08570) as described in the manufacturer's

331 protocol and Tilak and colleagues (2021b). Briefly, on Day 0, iPSCs were lifted with
332 Gentle Cell Dissociation Reagent, resuspended in embryoid body (EB) Seeding Medium,
333 and seeded in an ultra-low attachment, round bottom 96-well plate (Corning, Cat No. 7007)
334 at a density of 9,000 cells/well. EB Formation Medium was added on Days 2 and 4, and
335 on Day 5, EBs were transferred to ultra-low attachment 24-well plates (Corning, Cat No.
336 3473) containing Induction Medium for 48 hours. On Day 7, EBs were encased in droplets
337 of Matrigel on organoid embedding sheets (StemCell Technologies, Cat No. 08579), which
338 were allowed to polymerize at 37°C before being washed into ultra-low attachment 6-well
339 plates (Corning, Cat No. 3471) using 3 mL of Expansion Medium. On Day 10, the
340 Expansion Medium was replaced with Maturation Medium, and the plate was transferred
341 to an orbital shaker inside a 37°C, 5% CO_2 incubator. The media was changed three times
342 per week until Day 60, the beginning of the organoid co-culture assay.
343
344 *Organoid co-culture assay*
345 The organoid co-culture assay protocol was modified from Tilak and colleagues (2021b).
346 Tumorspheres were generated similar to above, except with 12,000 GFP-expressing U-87
347 cells seeded per well. Sixty (60)-day-old organoids were removed from the 6-well plate
348 and placed individually in 1.5 mL Eppendorf tubes, each containing 4 tumorspheres and
349 500 μL of Maturation Medium. Tubes were incubated at 37°C and 5% CO_2 inside 10 cm
350 dishes with the caps open to allow airflow during attachment, while maintaining a sterile
351 environment. After 48 hours, 50% of the media was replaced, and after 72 hours, organoids
352 with tumorsphere attached were gently removed from the tubes using a wide-bore pipette
353 and put back in 6-well plates on the orbital shaker for an additional 24 hours (for the 10-

354 day experiment) or 8 days (for the 3-day experiment), at which point cannflavin B (5 μM)
355 or DMSO was added to the well in a complete media change. Media containing cannflavin
356 B or DMSO was replaced every other day for the duration of the experiment. Fourteen days
357 after initiating the co-culture, all organoids were removed from the wells, washed three
358 times with PBS, and fixed in 4% paraformaldehyde overnight at 4°C. Organoids were
359 washed again with PBS and incubated in a 30% sucrose solution at 4°C for 4 days before
360 being embedded in a 7.5% gelatin, 10% sucrose solution and snap-frozen in dry ice
361 submerged in 95% ethanol. Twenty (20) μm sections were obtained using a cryostat (Leica,
362 CM1860), placed on Vectabond-coated slides (Vector Laboratories, Cat No. SP-1800-7),
363 and stored at -80°C until immunostaining.

364 For immunostaining, organoid sections were washed 3 times with PBS and blocked in
365 10% normal goat serum in PBS at room temperature for 30 minutes. Sections were
366 incubated overnight at 4°C in blocking solution containing primary antibodies (TUJ1 and
367 GFP, 1:1,000). Slides were washed again 3 times with PBS and incubated in Alexa Fluor-
368 488- or Alexa Fluor-594-conjugated secondary antibodies (Invitrogen, Cat Nos. A11039
369 and A11032) in 5% normal goat serum in PBS for 2 hours at room temperature. Slides
370 were washed 3 additional times in PBS, counterstained with DAPI, and cover-slipped with
371 ProLong Glass Antifade mounting reagent (Invitrogen, Cat No. P36984).

372 Captures were taken using a Nikon Eclipse Ti2-E microscope at 20× magnification.
373 Exposure for each channel was kept consistent between conditions. To analyze GFP-
374 positive U-87 cell infiltration in the corresponding cerebral organoid, the following steps
375 were followed: 1) the perimeter of the cerebral organoid was traced based on the TUJ1
376 signal, 2) a threshold of 100 was applied to the GFP channel to binarize pixels, and 3) the

377 number of GFP pixels was normalized to the total number of pixels in the TUJ1 channel to
378 provide the proportional count. For estimating tumorsphere area, a section from
379 approximately the middle of each tumorsphere to be analyzed was immunostained, and the
380 perimeter of the GFP signal was traced using the polygon selection tool in ImageJ software
381 by an individual blinded to the experimental conditions.
382
383 *Western blotting*
384 For western blot analysis, cells were seeded in 6-well plates and grown for 2 to 3 days
385 before treatment. After treatment, cells were collected with radioimmunoprecipitation
386 assay (RIPA) buffer (50 mM Tris [pH 8.0], 0.5% Igepal-CA-630, 0.1% SDS, 0.5%
387 deoxycholic acid, 1 mM EDTA, 300 mM NaCl), supplemented with Phosphatase Inhibitor
388 Cocktail 3 (Sigma-Aldrich, Cat No. P0044) and EDTA-free Protease Inhibitor Cocktail
389 (Sigma-Aldrich, Cat No. 11836170001), and homogenized using QIAshredder columns
390 (QIAGEN, Cat No. 79656). Concentration of all lysates was measured using Pierce BCA
391 Assay Kit (Thermo Fisher Scientific, Cat No. 23225), one volume of 2× Laemmli buffer
392 (100 mM tris-HCl [pH 6.8], 4% SDS, 0.15% bromophenol blue, 20% glycerol, 200 mM β-
393 mercaptoethanol) was added, samples were adjusted to an equal concentration, and finally
394 boiled for 5 minutes. A total of 15 μg of protein was run on a 10% SDS-PAGE gel and
395 transferred to a nitrocellulose membrane. Membranes were incubated in TBST (Tris-
396 buffered saline and 0.1% Tween 20) supplemented with 5% non-fat powdered milk for 30
397 min at room temperature, and then probed overnight with the intended primary antibody at
398 the following dilution: P-TrkB Y705 (1:1,000), P-AKT S473 (1:1,000), P-AKT T308
399 (1:1,000), pan-AKT (1:2,000), P-p44/p42 MAPK (1:1,000), p42 MAPK (1:1,000), and

400 GAPDH (1:20,000). The next day, membranes were washed with TBST, incubated with
401 the appropriate secondary antibody, and visualized using enhanced chemiluminescence
402 (ECL), according to the manufacturer's guidelines (Pierce, Thermo Fisher Scientific). Each
403 experiment was repeated three times.

404 The western blots were quantified as follows: First, equal amount of protein sample
405 was analyzed by SDS-PAGE for each biological replicate. Second, the exposure time of
406 the film to ECL was the same for each biological replicate. Third, the exposed films were
407 scanned using a HP LaserJet Pro M377dw scanner in grayscale at a resolution of 300 dpi.
408 Finally, protein expression was quantified using ImageJ software to determine the mean
409 grey value of the protein bands, with the background value subtracted. The pixel density
410 for all data was inverted by subtracting the mean grey value from 255. The final values of
411 each protein band were taken as a ratio over the corresponding loading control to provide
412 a normalized value for statistical analysis.

413

414 *Statistical analysis*

415 All statistical calculations were completed with Prism 10 (GraphPad Software, Boston,
416 MA, USA). No statistical methods were employed to predetermine the sample size of any
417 of the presented experiments. Student *t*-test or analysis of variance (ANOVA) plus Tukey's
418 post hoc test for multiple comparisons was performed where indicated. A value of $p \leq .05$
419 was considered statistically significant. No test for outliers was conducted, and no data
420 point was excluded. Unless mentioned otherwise, all results represent the mean ± SEM
421 from at least three independent experiments ($n = 3$). Sample size was estimated based on

422 previous studies of a similar nature (Lalonde et al., 2021; Holborn et al., 2023; Lau et al.,
423 2025).
424
425 **RESULTS**
426 *Cannflavin B decreases GBM cell viability*
427 The flavonol kaempferol and flavone apigenin have been shown to significantly reduce the
428 viability of different cancer cell types in the low micromolar concentration range after 24-
429 48 hours of exposure (e.g., Gao *et al.*, 2018; Tseng *et al.*, 2017). Except for the work of
430 Moreau and colleagues (2019) using mouse models of metastatic pancreatic cancer and the
431 study by Tomko and colleagues (2022), which reported a promising effect of cannflavin A
432 against bladder carcinoma cells, we know little about the impact of cannflavins on other
433 cancer types. This prompted us to thoroughly test the effect of cannflavin A and cannflavin
434 B on the viability of the A-172 and U-87 GBM cell lines. Importantly, we used the small-
435 molecule non-competitive TrkB antagonist ANA-12 (Cazorla et al., 2011) as a comparison
436 compound in this analysis because it has been reported to reduce A-172 cell viability in a
437 dose- and time-dependent manner (Pinheiro et al., 2017). Hence, this represents a relevant
438 reference measure that also connects with our recent publication demonstrating the
439 interference of cannflavins A and B on TrkB signaling in mouse primary cortical neurons
440 (Holborn et al., 2023).
441 As presented in **Figure 1**, applying cannflavin A and cannflavin B in the 1-20 μM
442 final concentration range to the culture media of either A-172 (**Fig. 1A-C**) and U-87 (**Fig.
443 1D-F**) cells produced similar mixed results. Specifically, no significant effect on viability
444 was detected using a resazurin reduction assay for cannflavin A at any concentration or

445 time-point, although a trend for reduced viability can be observed in A-172 cells with the
446 highest concentration (20 μM) at the 24-hour and 48-hour time-points. On the other hand,
447 cannflavin B produced a robust reduction in viability for both A-172 and U-87 cells, with
448 the most significant effect observed at higher concentrations (20 μM) and longer treatment
449 times (48 hours). Interestingly, ANA-12 in the 20-50 μM range also negatively affected
450 survival in both cell lines, with the notable difference that higher compound concentrations
451 were required to achieve an impact comparable to that of cannflavin B. This can be best
452 appreciated at 48 hours in A-172 cells, where 5 μM cannflavin B reduced viability below
453 50%, while ANA-12 at 10 μM had no statistically significant effect (estimated average cell
454 viability of 90%). The estimated IC50 for each of the compounds and time-points in this
455 experiment are presented in the **Supplementary Information**. Together, these results
456 establish that cannflavin B is more potent at affecting GBM cell survival than cannflavin
457 A and ANA-12.

458 To gain a broader view of the potency of cannflavin B towards U-87 cells, we next
459 performed a similar experiment with two structurally related flavones, namely chrysoeriol,
460 the non-prenylated synthesis precursor of cannflavins in the *C. sativa* plant (**Fig. S2A**, Rea
461 et al., 2019), and techtochrysin (**Fig. S2B**), an O-methylated flavone previously discovered
462 to have effects against SW480 and HCT116 colon cancer cells through inhibition of
463 Nuclear factor-κB (NF-κB) activity (Park et al., 2015). Interestingly, we found that the
464 direct application of chrysoeriol to the cell culture medium significantly reduced U-87 cell
465 viability, but only at a final concentration of 20 μM and for treatment times of 24-48 hours
466 (**Fig. S2C**). This result suggests that the prenyl group found at the 3' position of the flavone
467 B-ring that distinguishes cannflavin B from chrysoeriol contributes to the potency of the

468 latter molecule in this assay. The effect of techtochrysin, however, was the opposite of that
469 of chrysoeriol. Intriguingly, application of techtochrysin in the range of 5-40 μM for 24-
470 48 hours significantly enhanced the viability of U-87 cells. In summary, these experiments
471 reinforce the notion that cannflavin B exerts anti-survival effects on GBM cells at lower
472 concentrations and more rapidly than closely related flavones.

473 *Cannflavins A and B do not induce necrosis in GBM cells*

474 To assess the extent to which cannflavin B's observed impact on GBM cell viability could
475 be attributed to necrosis, we performed cell membrane integrity tests with the lactate
476 dehydrogenase (LDH) release assay. A-172 and U-87 cells treated with 10-20 μM
477 cannflavin A or cannflavin B for 24 hours presented minimal LDH release (**Fig. S3A, B**).
478 Specifically, application of cannflavin A resulted in 3.57% LDH release at 10 μM and
479 2.54% at 20 μM in A-172 cells, and 0.96% at 10 μM and 1.03% at 20 μM in U-87 cells.
480 For cannflavin B, LDH release was 4.43% at 10 μM and 5.38% at 20 μM in A-172 cells,
481 and 0.81% at 10 μM and 0.88% at 20 μM in U-87 cells. Those values are comparable to
482 those obtained with ANA-12 at 10 μM (2.01% for A-172 cells and 1.61% for U-87). In
483 summary, these results suggest that the adverse effect of cannflavin B on cell viability, as
484 assessed using the resazurin reduction method, is not due to necrotic cell death at the
485 specified concentrations and time points.

486

487 *Cannflavins A and B do not cause apoptosis in the low micromolar range*

488 Our following goals were to assess the effect of cannflavins A and B in the low micromolar
489 (1 to 10 μM) range on GBM's cell cycle, migration, and capacity to invade. Before
490 proceeding with those tests, though, we wanted to confirm that neither cannflavin A nor

491 cannflavin B causes widespread programmed cell death resulting in DNA fragmentation
492 after at least 24 hours of exposure. Using the highly sensitive TUNEL assay, we observed
493 that A-172 GBM cells treated with cannflavin A or cannflavin B at a final concentration of
494 10 μM for 24 hours did not produce a noticeable fluorescein signal indicative of apoptosis
495 (**Fig. S3C**). This negative result assures that any effect associated with cannflavins at a
496 concentration of 10 μM or lower, which will be identified next, is distinct from
497 programmed cell death.
498
499 *Effect of cannflavins on A-172 and U-87 cell cycle*
500 Various flavonoids have been demonstrated to affect the cell cycle of different cancer cell
501 types (e.g., Lin et al., 2015; Srivastava et al., 2016; Zhang et al., 2017). This led us to ask
502 whether cannflavins A and B, at concentrations that do not produce a rapid and significant
503 anti-viability effect on A-172 and U-87 cells, could alter their cell cycle. Flow cytometry
504 analysis showed that neither cannflavin A nor cannflavin B affected cell cycle phase after
505 24 hours of treatment in the concentration range of 1-5 μM (**Fig. 2**). Interestingly, the A-
506 172 and U-87 cell lines exhibited distinctive distributions of the cell cycle that remained
507 unchanged with treatment (G1 proportion for the DMSO control was 61.7% and 41.6%,
508 respectively). In both GBM cell lines, compared to the DMSO control, there was no
509 statistically significant change in the cell cycle phase upon cannflavin A or cannflavin B
510 treatment. These results demonstrate that cannflavins in the low micromolar range (1 to 10
511 μM) do not alter GBM cell cycle.
512
513 *Cannflavins limit GBM cell migration and invasion*

514 Invasion and metastasis are primarily responsible for mortality associated with solid tumors
515 (Li et al., 2025). This is the case for GBM, where rapid invasion and damaging infiltration
516 of the cancer cells into surrounding healthy brain tissue account for most of the poor
517 outcomes (Barbaro et al., 2022). Therefore, systematically assessing the action of
518 cannflavins on GBM cell migration and invasion is highly relevant.

519 To start, we completed an analysis of cell migration using a time-lapse scratch assay
520 in which cannflavin A (10 μM final concentration), cannflavin B (5 μM final
521 concentration), ANA-12 (10 μM final concentration), or DMSO alone was applied directly
522 to the culture media of A-172 cells. Cell migration into the scratch wound area was
523 monitored over 48 hours (**Fig. 3A** and **Supplementary Video**). Our data revealed striking
524 differences between wells treated with cannflavins and exposed to DMSO. First, analysis
525 of the binary area fraction over all time-points suggested a delayed wound closure in
526 inhibitor-treated conditions and more linear cell movement over time for the DMSO and
527 cannflavin A conditions compared to the cannflavin B and ANA-12 (**Fig. 3B**). Examining
528 next just the 24-hour and 48-hour time-points, we found that the normalized wound area
529 fraction was significantly lower for the three tested molecules compared to DMSO (**Fig.**
530 **3C**). Further, considering the data as a percentage of wound closure, significantly less area
531 was covered by cells after 24 hours and 48 hours exposure to cannflavin B, but only at 48
532 hours for cannflavin A (**Fig. 3D**). ANA-12 results in that analysis were not different
533 compared to DMSO. Finally, considering the number of individual cells detectable within
534 the wound area, significantly fewer were present at the end of the experiment for cannflavin
535 B (**Fig. 3E**).

536 Next, we performed a transwell assay to gauge the potential of cannflavin B to limit
537 A-172's capacity to invade when the cells are exposed to the molecule. A-172 cells were
538 pre-treated overnight (~16 hours) with 10 μM cannflavin B or DMSO and then plated on
539 Matrigel-coated inserts with the addition of fresh cannflavin B (10 μM). As presented in
540 **Figure 4**, the results from the transwell invasion assay revealed that exposure to cannflavin
541 B significantly reduced the number of cells that invaded through the Matrigel matrix,
542 resulting in a statistically significant reduction of more than 50% compared to the vehicle
543 control. This result supports that cannflavin B at a concentration of 10 μM effectively
544 inhibits GBM cell migration and invasion, providing initial evidence of its potential against
545 tumor progression.

546 Lastly, since U-87 cells have a strong tendency to aggregate and form tumor-like
547 spheroid formations (tumorspheres) in suspension culture, we leverage this attribute to
548 provide a different evaluation of the action of cannflavins A and B on the invasion ability
549 of these GBM cell subtypes. Specifically, we cultured U-87 as 3-dimensional (3D)
550 tumorspheres and then embedded those within a Matrigel matrix to measure how they
551 would progress in the outward direction (**Fig. 5A**). Interestingly, adding cannflavin A to
552 the culture media at a final concentration of 10 μM resulted in a significantly smaller radius
553 and area of tumorsphere outgrowth at the three examined times (**Fig. 5B, C**). For cannflavin
554 B, tumorspheres in wells treated at a final concentration of 5 μM presented a significantly
555 reduced area at 72 hours after the start of the experiment (**Fig. 5B**) and a smaller radius in
556 the 48-72 hours times (**Fig. 5C**). ANA-12, for its part, was minimally active in this assay
557 producing only a slight significant effect on radius at 72 hours (**Fig. 5C**). Taken together,
558 these three experiments provide strong evidence that cannflavins, particularly cannflavin

559 B, can produce rapid and sustained anti-migration and anti-invasion action against GBM
560 cells.
561
562 *Cannflavin B limits the growth and infiltration of U-87 GBM tumorspheres attached to*
563 *cerebral organoids*
564 Conventional pre-clinical studies for GBM consist of monolayer tumor cell cultures and
565 animal approaches, including xenografts and genetically engineered mouse models
566 (Gómez-Oliva et al., 2021; Haddad et al., 2021). However, these strategies encounter
567 significant obstacles in recapitulating the complexity of GBM, especially the variety of
568 tumor cellular states and the cancerous mass microenvironment. The use of brain organoids
569 derived from human pluripotent stem cells helps overcome some of those challenges and
570 provides exciting new ways to study GBM tumor formation and invasion in real time
571 (Linkous et al., 2019; Wang et al., 2023)—an approach that our group has used with
572 success in recent years (Tilak et al., 2021b; Lau et al., 2025). To test if cannflavin B could
573 produce therapeutically relevant effects in a more complex *in vitro* system, we conducted
574 a co-culture experiment where iPSC-derived cerebral organoids matured for 60 days were
575 mixed with U-87 tumorspheres expressing GFP (**Fig. 6A**). Our pool of co-culture
576 specimens was then divided in two groups: one where the U-87 tumorspheres attached and
577 grew unchallenged for 11 days followed by the application of cannflavin B at a final
578 concentration of 5 μM in the culture media for 3 days (Paradigm 1), and another (Paradigm
579 2) where the cancer cells attached and grew for 4 days and then 5 μM cannflavin B was
580 added for 10 days (**Fig. 6B**). Co-cultures treated with DMSO only were included for both
581 tests as control, and media change with fresh cannflavin B (5 μM) or DMSO was done

582 every other day for the duration of the experiment. As seen in fluorescence microscopy
583 captures of immunostained sections (**Figure 6C-F**), U-87 tumorspheres attached to
584 cerebral organoids in both paradigms. In the two DMSO control conditions (**Fig. 6C, E**), a
585 distinct intermingling between GBM cells expressing GFP and neurons, as revealed by
586 TUJ1 immunostaining, can be observed at the edge of the cerebral organoid where the
587 tumorsphere is attached. Interestingly, less GBM cell penetration into the organoids was
588 observed in the cannflavin B-treated wells in both tests (**Fig. 6D, F**). To quantify this
589 phenotype, we determined the proportion of pixels corresponding to the GFP signal (U-87
590 GBM cells) in their respective cerebral organoid section (**Fig. 6G, H**). Although this
591 analysis did not reveal statistical significance due to low GBM cell infiltration in some
592 DMSO control replicates, cannflavin B-treated samples consistently showed very little
593 GFP signal. Considering this fact, we consider this result highly consistent with other
594 findings demonstrating the efficacy of cannflavin B against GBM cells. Finally, although
595 the tumorsphere total area for corresponding sections was not statistically different between
596 the two conditions in the 3-day (Paradigm 1) experiment (**Fig. 6I**), we found that the U-87
597 tumorspheres were significantly smaller when cannflavin B was added for 10 days
598 (Paradigm 2, **Fig. 6J**). Together, these observations collected with a more physiologically
599 relevant model provide compelling additional data to support an effect of cannflavin B
600 against the ability of aggressive GBM cells to invade human brain-like tissue.
601
602 *Cannflavins A and B impact on TrkB signaling in GBM cells*
603 As mentioned previously, a study by Pinheiro and colleagues (2017) reported that the TrkB
604 inhibitor ANA-12 reduces the viability of A-172 cells, suggesting that the activity of this

605 RTK may be essential for the growth and survival of this GBM cell line. Since our previous
606 work using mouse primary cortical neurons also found that cannflavins A and B can
607 interfere with TrkB signaling (Holborn et al., 2023), we considered it necessary to gain
608 more information about the effect of cannflavins and ANA-12 on TrkB signaling in A-172
609 (**Fig. 7**) and U-87 (**Fig. 8**) cells to interpret our functional data. As expected, western blot
610 analysis revealed that application of cannflavin A at a final concentration of 20 μM (**Fig.**
611 **7A, B**) and cannflavin B at 10-20 μM (**Fig. 7F, G**) to the culture media of A-172 cells for
612 6 hours significantly reduced the phosphorylation of TrkB at tyrosine 705 (Y705), which
613 is in the catalytic domain and stimulates kinase activity of the receptor when
614 phosphorylated. Consistent with this result, ANA-12 at a final concentration of 10 μM also
615 significantly decreased phospho-TrkB Y705 signal (**Fig. 7B, G**). Interestingly, however,
616 our western blot data also revealed two unexpected and critical results. Firstly, key
617 downstream TrkB signaling effectors (i.e., p44/p42 MAPK and AKT) were unaffected by
618 cannflavins and ANA-12 in A-172 cells (**Fig. 7C-E, H-J**). Secondly, cannflavins and
619 ANA-12 did not impair TrkB phosphorylation and downstream signaling effectors in U-
620 87 cells, even at the highest tested concentration (**Fig. 8**). Together, these western blot data
621 force the critical conclusion that any positive results about GBM survival, migration, and
622 invasion presented above are most likely distinct from TrkB signaling impairment, whether
623 they were the result of cannflavins or ANA-12 treatment.
624

625 **DISCUSSION**

626 In this study, we employed various *in vitro* assays to characterize the phenotypic outcomes
627 of cannflavins A and B on the viability, cell cycle, migration, and invasion capacities of A-

628 172 and U-87 GBM cells. Of particular interest, our results show a consistent dose-
629 dependent decrease in cell viability in both lines when cannflavin B is added to the culture
630 media. No effect on cell cycle by either cannflavin molecule was detected, but we found
631 that both molecules can reliably limit tumor cell migration below the 10 μM concentration
632 and that cannflavin B has robust anti-invasive properties based on results from transwell
633 and tumorsphere assays. Together, these observations underscore the multifaceted
634 therapeutic potential of cannflavin B against this aggressive type of brain cancer.

635 Focusing first on our overall cell survival results, it is interesting to speculate about
636 why cannflavin B shows a higher effect against A-172 and U-87 cells than the other tested
637 flavonoids (i.e., cannflavin A, chrysoeriol, and techtochrysin). One key factor contributing
638 to this effect is certainly prenylation, which is considered to increase the lipophilicity of
639 flavonoids, thereby enhancing their affinity for biological membranes and improving their
640 interactions with target proteins (Xu et al., 2012; Yang et al., 2015). The reduced potency
641 of chrysoeriol, which is structurally similar to cannflavins A and B but lacks prenylation
642 attached to the B-ring (**Fig. S2A, C**), is consistent with this interpretation. That said, the
643 length and position of the prenyl side-chain are undoubtedly also critical, as we measured
644 greater bioactivity with cannflavin B, which has a single prenyl group, compared to
645 cannflavin A, which has two (**Fig. S1**). Finally, another structural-activity feature that may
646 explain other differences among flavonoids in our study is the B-ring hydroxylation
647 patterns. In fact, extensive evidence suggests that hydroxylation at specific positions can
648 markedly enhance bioactivity (Liu et al., 2022; Li et al., 2023). This detail most likely
649 contributed to the result we obtained in the techtochrysin test (Fig. S2B, D).

650 In addition, we conducted a western blot analysis to gain insights about the possible
651 molecular signaling changes induced by cannflavins that could produce the reported
652 cellular effects. However, the tested cannflavins and ANA-12 consistently reduced TrkB
653 phosphorylation at Y705 in A-172 cells, but this effect was not observed in U-87 cells. The
654 divergent TrkB phosphorylation responses observed in A-172 and U-87 cells likely reflect
655 differences in baseline endogenous TrkB expression (**Fig. S4**) and downstream pathway
656 coupling. U-87 cells are known to express lower levels of full-length TrkB than A-172
657 cells, which may explain their limited responsiveness. Most importantly, cannflavins and
658 ANA-12 had minimal effects on MAPK and AKT, which are well-known contributing
659 factors to cancer hallmarks, including growth, apoptosis, and invasion. These unexpected
660 results depart from our previous work on cannflavins A and B in mouse primary cortical
661 neurons (Holborn et al., 2023) and suggest that different molecular events, influenced by
662 cannflavins, are responsible for the migration and invasion disruptions observed in GBM
663 cells in this study. Therefore, future work is needed to elucidate the target engagement of
664 cannflavins in GBM cells. One unbiased strategy for this task could be to utilize the
665 Proteome Integral Solubility Alteration (PISA) assay, a high-throughput and mass-
666 spectrometry-based approach that leverages binding-dependent changes in protein
667 solubility to identify drug-target interactions (Gaetani et al., 2019; Gaetani and Zubarev,
668 2023).

669 On a separate note, an intriguing finding in our study concerns the increased viability
670 of U-87 cells exposed to techtochrysin (**Fig. S2B, D**)—a flavone molecule that had been
671 reported to suppress the growth of SW480 and HCT116 human colon cancer cells by
672 inhibiting NF-κB resulting in the expression of death receptors like DR3, DR4, and Fas

673 (Park et al., 2015). Although we cannot explain at this point why U-87 cells exposed to this
674 specific flavone produced an opposite effect to what has been reported with human colon
675 cancer cells, this bring to our attention the possibility that some of the anti-cancer
676 phenotypes associated with cannflavins A and B that we found may be linked to disruption
677 of the transcription factor NF-κB. Indeed, extensive research has implicated NF-κB in
678 various aspects of cancer formation, growth, treatment response, immune escape, and other
679 related processes (Taniguchi and Karin, 2018; Zhang et al., 2021; Khan et al., 2024). In
680 GBM and other gliomas, it has been reported for more than two decades that the aberrant
681 constitutive activity of this transcription factor contributes to disease initiation and
682 progression, including the invasion phenotype (Nagaai et al., 2002; Raychaudhuri et al.,
683 2004; Wang et al., 2004). Considering this, one tantalizing scenario is the disruption by
684 cannflavins of the constitutive signaling pathway that phosphorylates and promotes
685 degradation of IκBα by the ubiquitin-proteasome system, ultimately releasing NF-κB
686 dimers that translocate to the nucleus and modulate target gene expression that contributes
687 to disease progression (Cahill et al., 2016). While the present study did not directly evaluate
688 NF-κB activity, these findings raise the possibility that cannflavin B may influence NF-
689 κB–associated invasion programs. Future work incorporating NF-κB reporter assays and
690 transcriptomic profiling will be essential to define the signaling changes underlying the
691 anti-invasive effects observed here. If this is the case, it would be revealing to test the effect
692 of cannflavin B administration in xenograft or induced mouse models of GBM as used in
693 previous work targeting aberrant NF-κB activity (Friedmann-Morvinski et al., 2016).
694 Ultimately, this would provide a direct test of this hypothesis and additional pre-clinical
695 evidence to promote cannflavin B as a potentially valuable therapeutic agent against GBM.

696 Lastly, we present evidence that GFP-expressing U-87 cells migrating from a
697 tumorsphere can be challenged by cannflavin B at low μM levels as they infiltrate human
698 iPSC-derived cerebral organoids. Although we could not obtain precise quantitative
699 measures of GBM cell infiltration into the cerebral organoid structure using thin frozen
700 sections, we found that the tumorsphere size was significantly smaller after 10 days of
701 exposure to cannflavin B than after exposure to DMSO (vehicle control). This result calls
702 for a deeper investigation into the therapeutic value of cannflavin B against GBM or the
703 brain metastasis of other cancer types using live animal approaches, as mentioned above.
704 Corroborating the effectiveness of cannflavin B at limiting cancer progression with future
705 animal models would advance our research towards the design and proposal of a clinical
706 trial with human patients.

707 In conclusion, the distinctive ability of cannflavins, particularly cannflavin B, to
708 inhibit GBM cell migration and invasion, combined with their restrained cytotoxicity,
709 positions them as promising candidates for developing novel therapeutic strategies against
710 GBM (**Fig. S5**). Future studies should focus on validating these effects in animal models
711 to understand the pharmacokinetics, bioavailability, and therapeutic index of cannflavins.
712 Furthermore, exploring the synergistic impact of cannflavins with existing
713 chemotherapeutic agents or targeted therapies could provide valuable insights into their
714 potential as adjuvant treatments, particularly in overcoming drug resistance—a significant
715 challenge in the management of GBM. Combining cannflavins with agents like TMZ
716 (Stupp et al., 2005; Stupp et al., 2009; Fisher et al., 2013) or the anti-angiogenic agent
717 bevacizumab (Fu et al., 2023) could enhance their therapeutic efficacy by simultaneously
718 targeting multiple aspects of tumor growth and invasion.

DATA AVAILABILITY

All data collected for the study are available upon inquiry to the corresponding author.

CONSENT FOR PUBLICATION

Consent to publish the article has been obtained from all authors.

FUNDING

This work was supported by Mitacs (Mitacs Elevate Program, IT29490) and the Canadian Foundation for Innovation (CFI, 037755). J.H. was also supported by a Queen Elizabeth II Graduate Scholarship in Science and Technology.

CREDIT AUTHORSHIP CONTRIBUTION STATEMENT

Jennifer Holborn: Conceptualization, Data curation, Formal analysis, Funding acquisition, Investigation, Writing – original draft, **Hannah Robeson:** Data curation, Methodology, Writing – review & editing. **Ellis Chartley:** Formal analysis, Methodology, Writing – review & editing. **Tiana Gluscevic**: Data curation, Methodology. **Adina Borenstein:** Methodology. **Colby Perrin:** Methodology. **Begüm Alural:** Methodology. **Himain Perera:** Visualization, Writing – review & editing. **Tariq A. Akhtar:** Resources. **Nina Jones:** Resources, Writing – review & editing. **Jasmin Lalonde:** Conceptualization, Data curation, Funding acquisition, Supervision, Writing – original draft.

DECLARATION OF COMPETING INTEREST

The other authors declare that they have no known competing financial interests or personal relationships that could have appeared to influence the work reported in this paper.

ACKNOWLEDGMENTS

We wish to thank our lab colleagues for their help with this project.

HTTPS://WWW.EDITORIALMANAGER.COM/PHYPLU/.EMENTARY MATERIALS

Fig. S1 Cannflavin family members.

Fig. S2 LDH assay and TUNEL assay.

Fig. S3 Chrysoeriol and techtochrysin survival assay.

Fig. S4 Level of phospho-TrkB Y705 between A-172 and U-87 untreated cells.

Fig. S5 Graphical abstract.

Supplementary Table. Estimated IC50 for anti-survival effects of cannflavins and ANA-12.

Supplementary Video. Scratch migration assay video.

REFERENCES

Balakrishnan, S., Bhat, F. A., Raja Singh, P., Mukherjee, S., Elumalai, P., Das, S., Patra, C. R., Arunakaran, J., 2016. Gold nanoparticle–conjugated quercetin inhibits epithelial–mesenchymal transition, angiogenesis and invasiveness via EGFR/VEGFR-2-mediated pathway in breast cancer. Cell Prolif. 49, 678–697. https://doi.org/10.1111/cpr.12296.

Barbaro, M., Blinderman, C.D., Iwamoto, F.M., Kreisl, T.N., Welch, M.R., Odia, Y., Donovan L.E., Joanta-Gomez, A.E., Evans, K.A., Lassman, A.B., 2022. Causes of death and end-of-life care in patients with intracranial high-grade gliomas. Neurology. 98, e260-e266. https://doi:10.1212/WNL.0000000000013057.

Barrett, M.L., Gordon, D., Evans, F.J., 1985. Isolation from Cannabis sativa L. of cannflavin—a novel inhibitor of prostaglandin production. Biochem Pharmacol. 34, 2019–2024. http://doi:10.1016/0006-2952(85)90325-9.

Birzu C, French P, Caccese M, Cerretti G, Idbaih A, Zagonel V, Lombardi G., 2020. Recurrent glioblastoma: From molecular landscape to new treatment perspectives. Cancers (Basel). 13, 47. https://doi.org/10.3390/cancers13010047.

Cahill, K.E., Morshed, R.A., Yamini, B., 2016. Nuclear factor-κB in glioblastoma: insights into regulators and targeted therapy. Neuro Oncol. 2016 18, 329–339. https://doi.org/10.1093/neuonc/nov265.

Cazorla, M., Prémont, J., Mann, A., Girard, N., Kellendonk, C., Rognan, D., 2011. Identification of a low-molecular weight TrkB antagonist with anxiolytic and antidepressant activity in mice. J. Clin. Invest. 121, 1846–1857. https://doi:10.1172/JCI43992.

779 Cheng, W.Y., Chiao, M.T., Liang, Y.J., Yang, Y.C., Shen, C.C., Yang, C.Y., 2013.
780 Luteolin inhibits migration of human glioblastoma U-87 MG and T98G cells through
781 downregulation of Cdc42 expression and PI3K/AKT activity. Mol. Biol. Rep. 40,
782 5315–5326. https://doi.org/10.1007/s11033-013-2632-1.
783 Choi, E.J., Bae, S.M., Ahn, W.S., 2008. Antiproliferative effects of quercetin through cell
784 cycle arrest and apoptosis in human breast cancer MDA-MB-453 cells. Arch. Pharm.
785 Res. 31, 1281–1285. https://doi.org/10.1007/s12272-001-2107-0.
786 Friedmann-Morvinski, D., Narasimamurthy, R., Xia, Y., Myskiw, C., Soda, Y., Verma,
787 I.M., 2016. Targeting NF-κB in glioblastoma: A therapeutic approach. Sci. Adv. 2,
788 e1501292. https://doi.org/10.1126/sciadv.1501292.
789 Eggers, C., Fujitani, M., Kato, R., Smid, S., 2019. Novel cannabis flavonoid, cannflavin
790 A displays both a hormetic and neuroprotective profile against amyloid β-mediated
791 neurotoxicity in PC12 cells: Comparison with geranylated flavonoids, mimulone and
792 diplacone. Biochem. Pharmacol., 169. https://doi.org/10.1016/j.bcp.2019.08.011.
793 Erdogan, S., Doganlar, O., Doganlar, Z.B., Serttas, R., Turkekul, K., Dibirdik, I., Bilir,
794 A., 2016. The flavonoid apigenin reduces prostate cancer CD44+ stem cell survival
795 and migration through PI3K/Akt/NF-κB signaling. Life Sci. 162, 77–86.
796 https://doi.org/10.1016/j.lfs.2016.08.019.
797 Fisher J.P., Adamson D.C., 2021. Current FDA-approved therapies for high-grade
798 malignant gliomas. Biomedicines. 9, 324.
799 https://doi.org/10.3390/biomedicines9030324.

800 Fu., M., Zhou, Z., Huang, X., Chen, Z., Zhang, L., Zhang, J., Hua. W., Mao, Y., 2023.
801 Use of Bevacizumab in recurrent glioblastoma: a scoping review and evidence map.
802 BMC Cancer. 23, 544. https://doi.org/10.1186/s12885-023-11043-6.
803 Gaetani, M., Sabatier, P., Saei, A.A., Beusch, C.M., Yang, Z., Lundström, S.L., Zubarev,
804 R.A., 2019. Proteome integral solubility alteration: A high-throughput proteomics
805 assay for target deconvolution. J. Proteome Res. 18, 4027–4037.
806 https://doi.org/10.1021/acs.jproteome.9b00500.
807 Gaetani, M., Zubarev, R.A., 2023. Proteome Integral Solubility Alteration (PISA) for
808 high-throughput ligand target deconvolution with increased statistical significance
809 and reduced sample amount. Methods Mol. Biol. 2554, 91–106.
810 https://doi.org/10.1007/978-1-0716-2624-5_7.
811 Gao, X., Wang, B., Wei, X., Men, K., Zheng, F., Zhou, Y., Zheng, Y., Gou, M., Huang,
812 M., Guo, G., Huang, N., Qian, Z., Wei, Y., 2012. Anticancer effect and mechanism
813 of polymer micelle-encapsulated quercetin on ovarian cancer. Nanoscale, 4, 7021–
814 7030. https://doi.org/10.1039/c2nr32181e.
815 Gao, Y., Yin, J., Rankin, G.O., Chen, Y.C., 2018. Kaempferol induces G2/M cell cycle
816 arrest via checkpoint kinase 2 and promotes apoptosis via death receptors in human
817 ovarian carcinoma A2780/CP70 cells. Molecules, 23, 1095.
818 https://doi.org/10.3390/molecules23051095.
819 Gómez-Oliva, R., Domínguez-García, S., Carrascal, L., Abalos-Martínez, J., Pardillo-
820 Díaz, R., Verástegui, C., Castro, C., Nunez-Abades, P., Geribaldi-Dolbán, N., 2021.
821 Evolution of experimental models in the study of glioblastoma: Toward finding

822 efficient treatments. Front. Oncol., 10, 614295.
823 https://doi:10.3389/fonc.2020.614295.
824 Haddad, A.F., Young, J.S., Amara, D., Berger, M.S., Raleigh, D.R., Aghi, M., Butowski,
825 N.A., 2021. Mouse models of glioblastoma for the evaluation of novel therapeutic
826 strategies. Neurooncol. Adv., **b**, vdab100. https://doi:10.1093/noajnl/vdab100.
827 Holborn J, Walczyk-Mooradally A, Perrin C, Alural B, Aitchison C, Borenstein A, Jones
828 N, Khokhar J.Y., Akhtar T.A., Lalonde J., 2023. Interference of neuronal TrkB
829 signaling by the cannabis-derived flavonoids cannflavins A and B. Phytomed. Plus.
830 3, 100410. https://doi.org/10.1016/j.phyplu.2023.100410.
831 Huang, L., Jin, K., Lan, H., 2019. Luteolin inhibits cell cycle progression and induces
832 apoptosis of breast cancer cells through downregulation of human telomerase reverse
833 transcriptase. Oncol. Lett. 17, 3842–3850. https://doi.org/10.3892/ol.2019.10052.
834 Jo, E., Park, S.J., Choi, Y.S., Jeon, W.K., Kim, B.C., 2015. Kaempferol suppresses
835 transforming growth factor-β1-induced epithelial-to-mesenchymal transition and
836 migration of A549 lung cancer cells by inhibiting Akt1-mediated phosphorylation of
837 Smad3 at threonine-179. Neoplasia. 17, 525–537.
838 https://doi.org/10.1016/j.neo.2015.06.004.
839 Johnson, D.R., O'Neill, B.P., 2012. Glioblastoma survival in the United States before and
840 during the temozolomide era. J. Neuro-Oncol. 107, 359–364.
841 https://doi.org/10.1007/s11060-011-0749-4.
842 Khan, A., Zhang, Y., Ma, N., Shi, J., Hou, Y., 2024 NF-κB role on tumor proliferation,
843 migration, invasion and immune escape. Cancer Gene Ther. 31, 1599–1610.
844 https://doi.org/10.1038/s41417-024-00811-6.

845 Kim, S. H., Yoo, E.S., Woo, J.S., Han, S.H., Lee, J.H., Jung, S.H., Kim, H.J., Jung, J.Y.,
846 2019. Antitumor and apoptotic effects of quercetin on human melanoma cells
847 involving JNK/P38 MAPK signaling activation. Eur. J. Pharmacol. 860:172568.
848 https://doi.org/10.1016/j.ejphar.2019.172568.
849 Lalonde, J., Reis, S.A., Sivakumaran, S., Holland, C.S., Wesseling, H., Sauld, J., Alural,
850 B., Zhao, W.N., Steen, J., Haggarty, S.J., 2017. Chemogenomic analysis reveals key
851 role for lysine acetylation in regulating Arc protein stability. Nat. Commun. 8:1659.
852 https://doi.org/10.1038/s41467-017-01750-7.
853 Lau, H.R., Alural, B., Martin, C.E., New, L.A., Smith, H.S., Tilak, M., Banerjee, S.L.,
854 Robeson, H.N., Bisson, N., Gingras, A.C., Lalonde J, Jones, N., 2025. ShcD adaptor
855 protein drives invasion of triple-negative breast cancer cells by aberrant activation of
856 EGFR signaling. Mol. Oncol. Mar. 28, https://doi.org/10.1002/1878-0261.70022.
857 Lee, W.J., Hsiao, M., Chang, J.L., Yang, S.F., Tseng, T.H., Cheng, C.W., Chow, J.M.,
858 Lin, K.H., Lin, Y.W., Liu, C.C., Lee, L.M., Chien, M.H., 2015. Quercetin induces
859 mitochondrial-derived apoptosis via reactive oxygen species-mediated ERK
860 activation in HL-60 leukemia cells and xenograft. Arch. Toxicol. 89, 1103–1117.
861 https://doi.org/10.1007/s00204-014-1300-0.
862 Li, Y., Liu, F., Cai, Q., Deng, L., Ouyang, Q., Zhang, X.H.F., Zheng, J., 2025. Invasion
863 and metastasis in cancer: molecular insights and therapeutic targets. Signal
864 Transduct. Target. Ther. 10, 57. https://doi.org/10.1038/s41392-025-02148-4.
865 Li, S., Yan, T., Deng, R., Jiang, X., Xiong, H., Wang, Y., Yu, Q., Wang, X., Chen, C.,
866 Zhu, Y., 2017. Low dose of kaempferol suppresses the migration and invasion of

867 triple-negative breast cancer cells by downregulating the activities of RhoA and
868 Rac1. Onco Targets Ther. 10, 4809–4819. https://doi.org/10.2147/OTT.S140886.
869 Li, X., Xu, R., Ni, T., 2023. Effects of B-ring structures on binding behavior of flavonols
870 with proteins: Experimental and molecular docking approaches. J Mol Struct. 1287,
871 135614. https://doi.org/10.1016/j.molstruc.2023.135614.
872 Lin, C.H., Chang, C.Y., Lee, K.R., Lin, H.J., Chen, T.H., Wan, L., 2015. Flavones inhibit
873 breast cancer proliferation through the Akt/FOXO3a signaling pathway. BMC
874 Cancer. 15, 958. https://doi.org/10.1186/s12885-015-1965-7.
875 Linkous, A., Balamatsias, D., Snuderl, M., Edwards, L., Miyaguchi, K., Milner, T.,
876 Reich, B., Cohen-Gould, L., Storaska, A., Nakayama, Y., Schenkein, E., Singhania,
877 R., Cirigliano, S., Magdeldin, T., Lin, Y., Nanjangud, G., Chadalavada, K., Pisapia,
878 D., Liston, C., Fine, H.A., 2019. Modeling Patient-Derived Glioblastoma with
879 Cerebral Organoids. Cell Rep., 26, 3203–3211.
880 Liu, L., Qian, J., Li, J., Xing, M., Grierson, D., Sun, C., Xu, C., Li, X., Chen, K., 2022.
881 Hydroxylation decoration patterns of flavonoids in horticultural crops: chemistry,
882 bioactivity, and biosynthesis. Hortic Res. 9, uhab068.
883 https://doi.org/10.1093/hr/uhab068.
884 Moreau, M., Ibeh, U., Decosmo, K., Bih, N., Yasmin-Karim, S., Toyang, N., Lowe, H.,
885 Ngwa, W., 2019. Flavonoid derivative of cannabis demonstrates therapeutic potential
886 in preclinical models of metastatic pancreatic cancer. Front. Oncol. 9, 660.
887 https://doi.org/10.3389/fonc.2019.00660.
888 Nagai, S., Washiyama, K., Kurimoto, M., Takaku, A., Endo, S., Kumanishi, T., 2002.
889 Aberrant nuclear factor-kB activity and its participation in the growth of human

890 malignant astrocytoma. J. Neurosurg. 96, 909–917.
891 https://doi.org/10.3171/jns.2002.96.5.0909.
892 Ostrom, Q.T., Patil, N., Cioffi, G., Waite, K., Kruchko, C., Barnholtz-Sloan J.S., 2020.
893 CBTRUS Statistical Report: Primary brain and other central nervous System tumors
894 diagnosed in the United States in 2013–2017. Neuro-Oncol., 22, iv1–iv96.
895 https://doi.org/10.1093/neuonc/noaa200.
896 Panche, A.N., Diwan, A.D., Chandra, S.R., 2016. Flavonoids: An overview. J. Nutr.
897 Sci. 5, e47. https://doi:10.1017/jns.2016.41.
898 Park, M.H., Hong, J.E., Park, E.S., Yoon, H.S., Seo, D.W., Hyun, B.K., 2015. Anticancer
899 effect of tectochrysin in colon cancer cell via suppression of NF-kappaB activity and
900 enhancement of death receptor expression. Mol. Cancer. 14:124
901 https://doi:10.1186/s12943-015-0377-2.
902 Pinheiro, K. V., Alves, C., Buendia, M., Gil, M. S., Thomaz, A., Schwartsmann, G., De
903 Farias, C. B., & Roesler, R., 2017. Targeting tyrosine receptor kinase B in gliomas.
904 Neuro. Oncol. 19, 138–139. https://doi.org/10.1093/neuonc/now199.
905 Pratheeshkumar, P., Budhraja, A., Son, Y.O., Wang, X., Zhang, Z., Ding, S., Wang, L.,
906 Hitron, A., Lee, J.C., Xu, M., Chen, G., Luo, J., Shi, X., 2012. Quercetin inhibits
907 angiogenesis mediated human prostate tumor growth by targeting VEGFR-2
908 regulated AKT/mTOR/P70S6K signaling pathways. PLoS ONE, 7, e47516.
909 https://doi.org/10.1371/journal.pone.0047516.
910 Raychaudhuri, B., Han, Y., Lu, T., Vogelbaum, M.A., 2007. Aberrant constitutive
911 activation of nuclear factor kappaB in glioblastoma multiforme drives invasive
912 phenotype. J. Neurooncol. 85, 39–47. https://doi.org/10.1007/s11060-007-9390-7.

913 Rea, K.A., Casaretto, J.A., Al-Abdul-Wahid, M.S., Sukumaran, A., Geddes-McAlister, J.,
914 Rothstein, S.J., & Akhtar, T.A., 2019. Biosynthesis of cannflavins A and B from
915 Cannabis sativa L. *Phytochemistry*, *164*, 162–171.
916 https://doi.org/10.1016/j.phytochem.2019.05.009.
917 Srivastava, S., Somasagara, R.R., Hegde, M., Nishana, M., Tadi, S.K., Srivastava, M.,
918 Choudhary, B., Raghavan, S.C., 2016. Quercetin, a natural flavonoid interacts with
919 DNA, arrests cell cycle and causes tumor regression by activating mitochondrial
920 pathway of apoptosis. Sci. Rep. 6, 24049. https://doi.org/10.1038/srep24049.
921 Stupp, R., Mason, W.P., Bent, M.J. van den, Weller M., Fisher, B., Taphoorn, M.J.B.,
922 Belanger, K., Brandes, A.A., Marosi, C., Bogdahn, U., Curschmann, J., Janzer, R.C.,
923 Ludwin, S.K., Gorlia, T., Allgeier, A., Lacombe, D., Cairncross, J.G., Eisenhauer, E.,
924 Mirimanoff, R.O., European Organisation for Research and Treatment of Cancer
925 Brain Tumor and Radiotherapy Groups; National Cancer Institute of Canada Clinical
926 Trials Group., 2005. Radiotherapy plus concomitant and adjuvant temozolomide for
927 glioblastoma. N. Engl. J. Med. 2352, 987–996.
928 https://doi.org/10.1056/nejmoa043330.
929 Stupp, R., Hegi, M.E., Mason, W.P., Bent, M.J. van den, Taphoorn, M.J., Janzer, R.C.,
930 Ludwin, S.K., Allgeier, A, Fisher, B., Belanger, K., Hau, P., Brandes, A.A.,
931 Gijtenbeek, J., Marosi, C., Vecht, C.J., Mokhtari, K., Wesseling, P., Villa, S.,
932 Eisenhauer, E., Gorlia, T., Weller, M., Lacombe, D., Cairncross, J.G., Mirimanoff,
933 R.O; European Organisation for Research and Treatment of Cancer Brain Tumour
934 and Radiation Oncology Groups; National Cancer Institute of Canada Clinical Trials
935 Group, 2009. Effects of radiotherapy with concomitant and adjuvant temozolomide

936 versus radiotherapy alone on survival in glioblastoma in a randomised phase III
937 study: 5-year analysis of the EORTC-NCIC trial. Lancet Oncol. 10, 459–466.
938 https://doi.org/10.1016/s1470-2045(09)70025-7.
939 Taniguchi, K., Karin, M., 2018. NF-κB, inflammation, immunity and cancer: coming of
940 age. Nat. Rev. Immunol. 18, 309–324. https://doi.org/10.1038/nri.2017.142.
941 Tilak, M., Alural, B., Holborn, J., Lalonde, J., Jones, N., 2021a. Receptor tyrosine kinase
942 signaling and targeting in glioblastoma. Int. J. Mol. Sci. 22, 1831.
943 https://doi:10.3390/ijms22041831.
944 Tilak, M., Alural, B., Wismer, S.E., Brasher, M.I., New, L.A., Sheridan, S.D., Perlis,
945 R.H., Coppolino, M.G., Lalonde, J., Jones, N., 2021b. Adaptor protein ShcD/SHC4
946 interacts with tie2 receptor to synergistically promote glioma cell invasion. Mol.
947 Cancer Res. 19, 757–770. https://doi.org/10.1158/1541-7786.MCR-20-0188.
948 Tomko, A.M., Whynot, E.G., Dupré, D.J., 2022. Anti-cancer properties of cannflavin A
949 and potential synergistic effects with gemcitabine, cisplatin, and cannabinoids in
950 bladder cancer. J. Cannabis Res. 4, 41. https://doi.org/10.1186/s42238-022-00151-y.
951 Tseng, T.H., Chien, M.H., Lin, W.L., Wen, Y.C., Chow, J.M., Chen, C.K., Kuo, T.C.,
952 Lee, W.J., 2017. Inhibition of MDA-MB-231 breast cancer cell proliferation and
953 tumor growth by apigenin through induction of G2/M arrest and histone H3
954 acetylation-mediated p21WAF1/CIP1 expression. Environ. Toxicol. 32, 434–444.
955 https://doi.org/10.1002/tox.22247.
956 Vinci, M., Box, C., Eccles, S.A., 2015. Three-dimensional (3D) tumor spheroid invasion
957 assay. J. Vis. Exp. 99, e52686. https://doi.org/10.3791/52686.

958 Wang, X., Sun, Y., Zhang, D.Y., Ming, G., Song, H., 2023. Glioblastoma modeling with
959 3D organoids: progress and challenges. Oxf. Open Neurosci. 2, kvad008.
960 https://doi:10.1093/oons/kvad008.
961 Wang, H., Wang, H., Zhang, W., Huang, H.J., Liao, W.S., Fuller, G.N. 2004. Analysis of
962 the activation status of Akt, NFkappaB, and Stat3 in human diffuse gliomas. Lab
963 Invest. 84, 941–951. https://doi.org/10.1038/labinvest.3700123.
964 Weller M, Cloughesy T, Perry J.R., Wick W., 2013. Standards of care for treatment of
965 recurrent glioblastoma—are we there yet? Neuro Oncol. 15, 4–27.
966 https://doi.org/10.1093/neuonc/nos273.
967 Werz, O., Seegers, J., Schaible, A.M., Weinigel, C., Barz, D., Koeberle, A., Allegrone,
968 G., Pollastro, F., Zampieri, L., Grassi, G., Appendino, G., 2014. Cannflavins from
969 hemp sprouts, a novel cannabinoid-free hemp food product, target microsomal
970 prostaglandin E_2 synthase-1 and 5-lipoxygenase. PharmaNutrition. 2, 53–60.
971 https://doi.org/10.1016/j.phanu.2014.05.001.
972 Xu, M. J., Wu, B., Ding, T., Chu, J. H., Li, C. Y., Zhang, J., Wu, T., Wu, J., Liu, S. J.,
973 Liu, S. L., Ju, W. Z., Li, P., 2012. Simultaneous characterization of prenylated
974 flavonoids and isoflavonoids in Psoralea corylifolia L. by liquid chromatography
975 with diode-array detection and quadupole time-of-flight mass spectrometry. Rapid
976 Commun. Mass Spectrom. 26, 2343–2358. https://doi.org/10.1002/rcm.6361.
977 Yang, X., Jiang, Y., He, J., Sun, J., Chen, F., Zhang, M., Yang, B., 2015. Prenylated
978 flavonoids, promising nutraceuticals with impressive biological activities. Trends
979 Food Sci. Technol. 44, 93e104. https://doi.org/10.1016/j.tifs.2015.03.007.

980 Zhang, Q., Cheng, G., Qiu, H., Wang, Y., Wang, J., Xu, H., Zhang, T., Liu, L., Tao, Y.,
981 Ren, Z., 2017. Expression of prostate stem cell antigen is downregulated during
982 flavonoid-induced cytotoxicity in prostate cancer cells. Exp. Ther. Med. 14, 1795–
983 1801. https://doi.org/10.3892/etm.2017.4638.
984 Zhang, T., Ma, C., Zhang, Z., Zhang, H., Hu, H., 2021 NF-κB signaling in inflammation
985 and cancer. MedComm. 2, 618–653. https://doi.org/10.1002/mco2.104.
986 Zhu, L., Xue, L., 2019. Kaempferol suppresses proliferation and induces cell cycle arrest,
987 apoptosis, and DNA damage in breast cancer cells. Oncol. Res. 27, 629–634.
988 https://doi.org/10.3727/096504018X15228018559434.
989

990 **FIGURE 1**

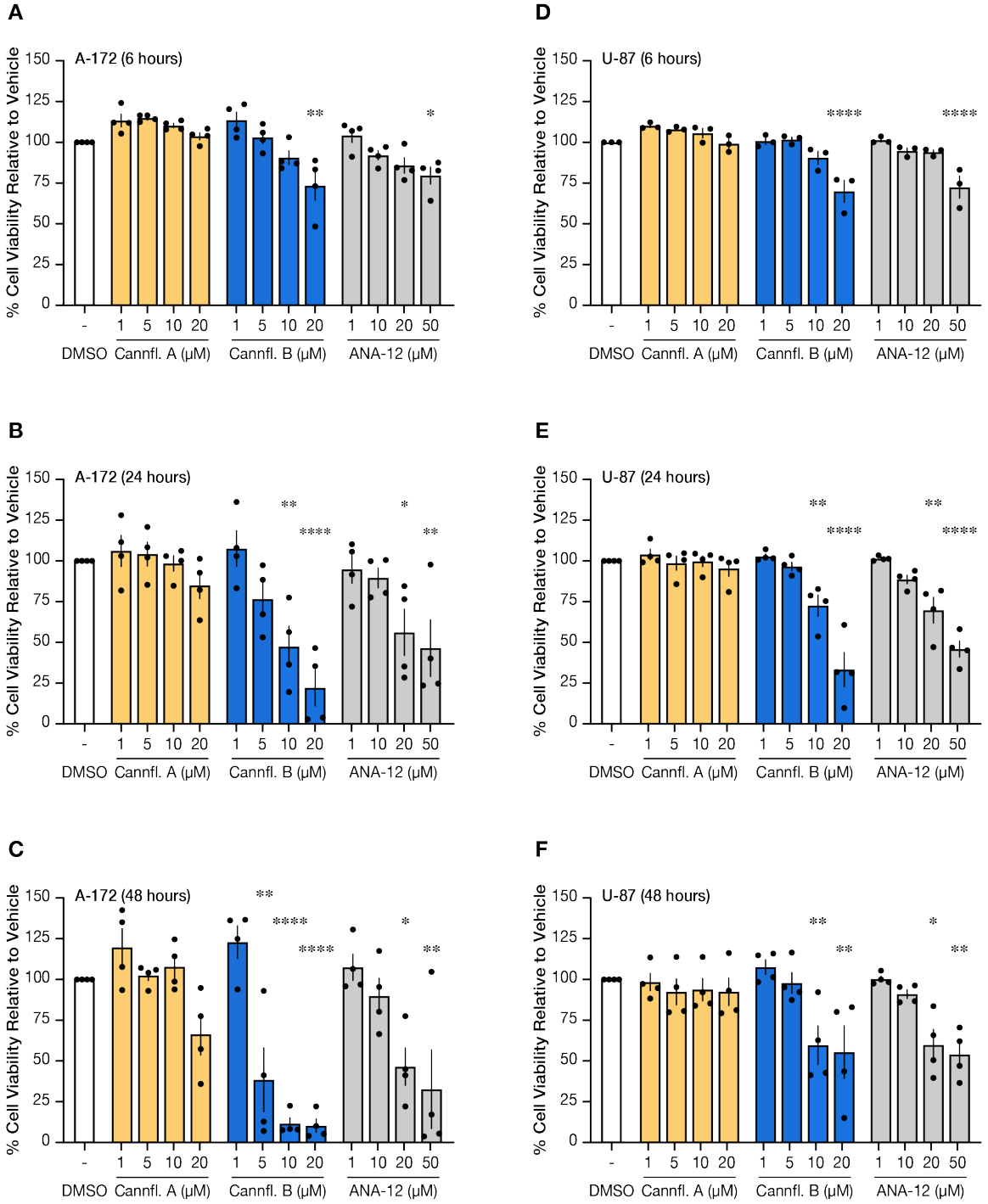

991

992 **Figure 1.** Cannflavin B reduces GBM cell viability. A172 **(A-C)** and U-87 **(D-F)** cells

993 were treated with increased concentrations of cannflavin A (1-20 μM), cannflavin B (1-20

994 μM), or ANA-12 (1-50 μM) and cell viability was measured at 24-, 48-, and 72-hour time-

995 points using the resazurin reduction assay. DMSO was used as a vehicle control.
996 Application of cannflavin B and ANA-12, but not cannflavin A, reduced the viability of
997 both A-172 and U-87 GBM cells in a dose- and time-dependent manner. A one-way
998 ANOVA was used to analyze the data from each cell line, treatment, and time point
999 independently with DMSO as the reference control. Tukey's honestly significant
1000 difference (HSD) post hoc test: * $p < 0.05$, ** $p < 0.01$, *** $p < 0.001$, **** $p < 0.0001$.
1001 Graphs represent mean ± SEM (n = 3-4).

1002 **FIGURE 2**

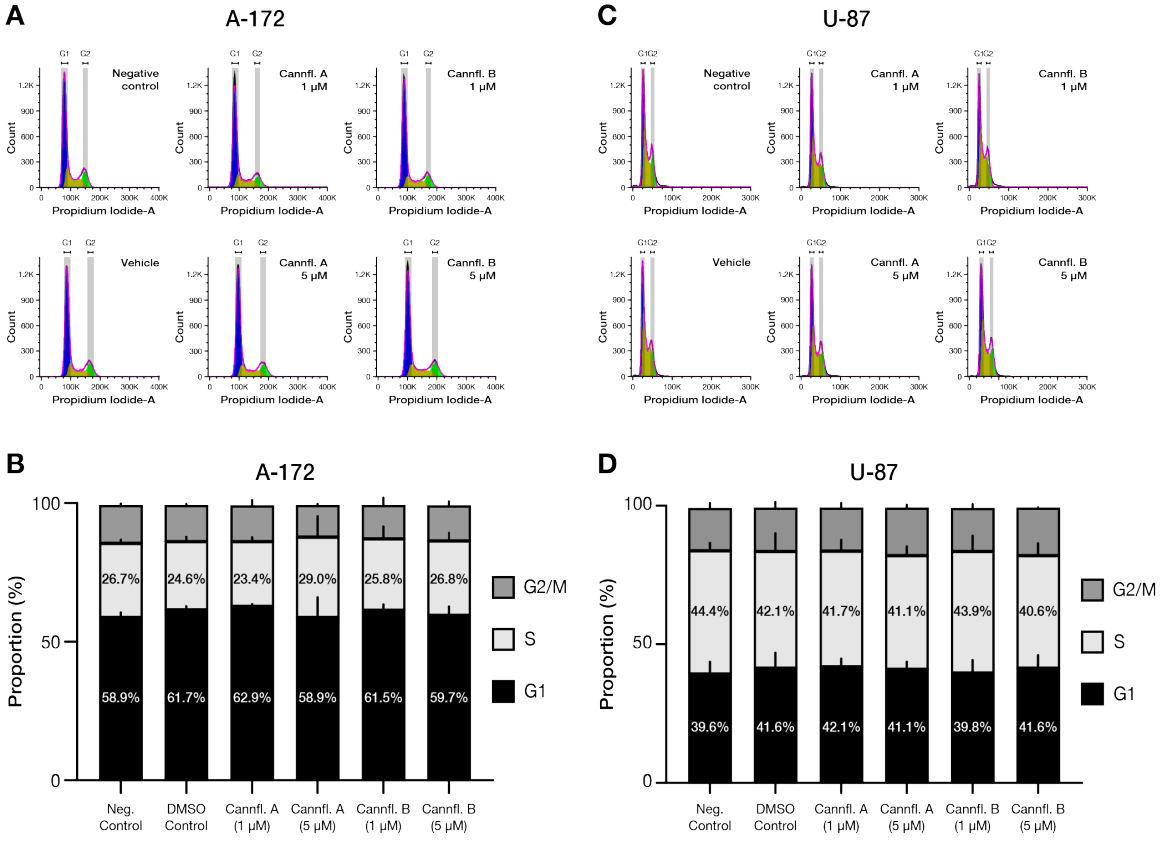

1003

1004 **Figure 2. Cannflavins A and B did not affect cell cycle distribution in GBM cell lines.**

1005 A-172 **(A-B)** and U-87 **(C-D)** DNA content was determined by gating on the G1, S, and

1006 G2/M phases using flow cytometry and analyzed using the Watson Pragmatic algorithm to

1007 distribute cell cycle phases. A172 **(B)** and U-87 **(D)** cell cycle data are expressed as mean

1008 ± SEM (n = 3).

1009 **FIGURE 3**

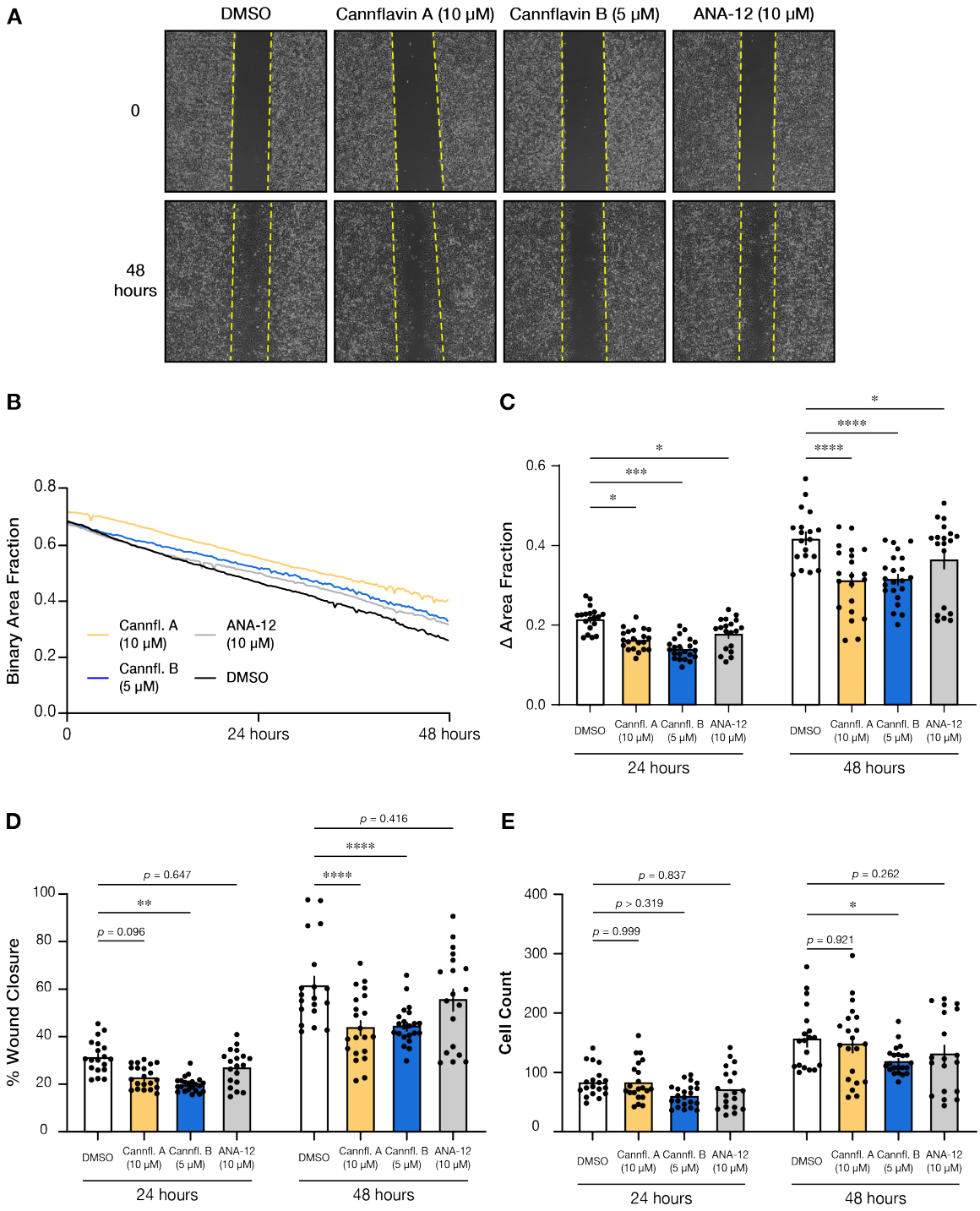

1010

1011 **Figure 3.** Cannflavins A and B suppress A-172 cell migration. **(A)** Representative phase-

1012 contrast images of scratch assay showing A-172 GBM cancer cells within a gap created

1013 with a pipette tip at 0 hour and 48 hours. Dashed yellow lines indicate the initial wound

edges. **(B)** Quantification of the binary wound area fraction over time, showing delayed wound closure in inhibitor-treated conditions. **(C)** Normalized wound area fraction at 24 hours and 48 hours. A two-way ANOVA reveals a significant effect of time ($F_{1,218} = 133.3$, $p < 0.0001$) as well as treatment ($F_{3,218} = 18.37$, $p < 0.0001$). There is no significant interaction between time and treatment ($F_{3,218} = 2.094$, $p = 0.1019$). Post hoc comparisons between DMSO control and each treatment means were conducted using Dunnett's multiple comparisons. All treatments at all time points produced a significant reduction in cell migration. **(D)** Percentage of wound closure at 24 hours and 48 hours. A two-way ANOVA reveals a significant effect of time ($F_{1,218} = 104.2$, $p < 0.0001$) as well as treatment ($F_{3,218} = 16.45$, $p < 0.0001$). There is no significant interaction between time and treatment ($F_{3,218} = 1.885$, $p = 0.133$). Post hoc comparisons between DMSO control and each treatment means were conducted using Dunnett's multiple comparisons. Cannflavin B significantly limited closure at both time points, while cannflavin A was significant only at 48 hours. ANA-12 did not cause a significant effect. **(E)** Total cell counts within the imaging field at 24 hours and 48 hours. A two-way ANOVA reveals a significant effect of time ($F_{1,154} = 92.25$, $p < 0.0001$) as well as treatment ($F_{3,154} = 4.46$, $p = 0.0049$). There is no significant interaction between time and treatment ($F_{3,154} = 0.2556$, $p = 0.8573$). Post hoc comparisons between DMSO control and each treatment means were conducted using Dunnett's multiple comparisons. Significantly less cells were found in the wound area with cannflavin B at 48 hours. No other comparisons were significantly different. All data represented as mean ± SEM (3 biological replicates with 6-8 images per well; * $p < 0.05$, ** $p < 0.01$, *** $p < 0.001$, **** $p < 0.0001$).

1036 **FIGURE 4**

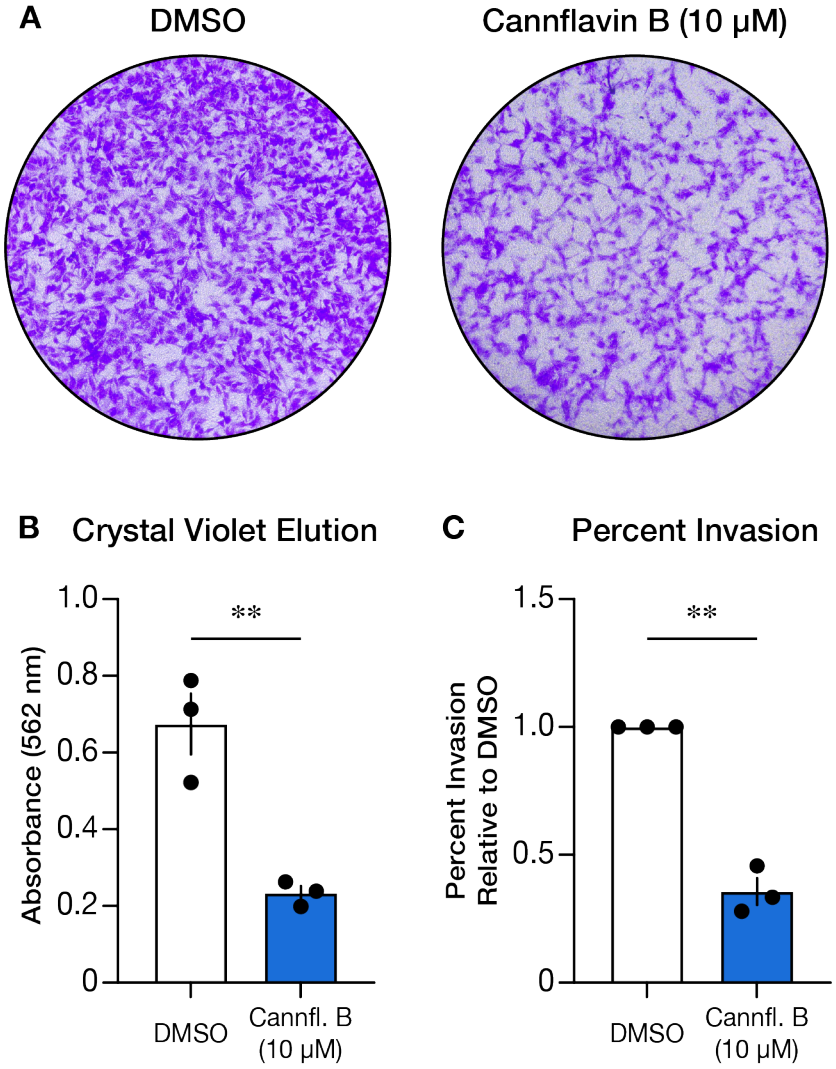

1037

1038 **Figure 4. Cannflavin B inhibits A-172 glioblastoma cell invasion in a transwell assay.**
1039 **(A)** Representative images of stained migrated A-172 cells following treatment with
1040 DMSO or cannflavin B (10 μM). **(B)** Quantification of migration using crystal violet
1041 elution measured by absorbance at 562 nm. **(C)** Percent invasion between DMSO control
1042 and cannflavin B, showing a significant reduction in cannflavin B-treated cells. Data
1043 represent mean ± SEM, with statistical significance determined by an unpaired two-tailed
1044 *t*-test (** $p < 0.01$).

1045 **FIGURE 5**

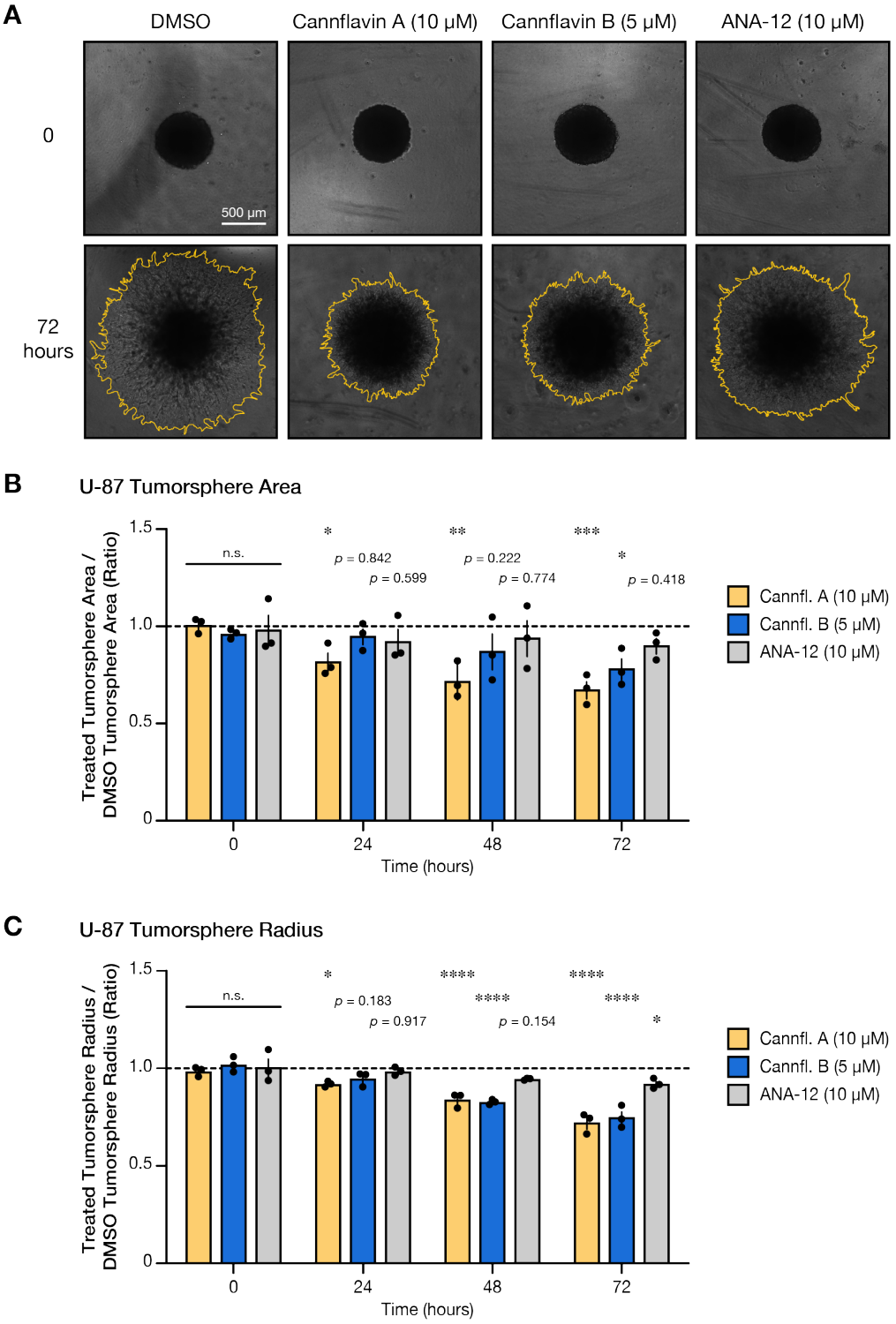

1046

1047 **Figure 5.** Cannflavins A and B inhibit the outgrowth of U-87 tumorspheres. **(A)**

1048 Representative phase-contrast images of U-87 tumorspheres at 0 hour and 72 hours post-

1049 treatment with DMSO (vehicle), ANA-12 (10 μM), cannflavin A (10 μM), or cannflavin
1050 B (5 μM) in a tumorsphere invasion assay. Scale bar: 500 μm. The white outline indicates
1051 the borders of tumorsphere outgrowth. **(B)** Quantification of relative tumorsphere area
1052 expansion over time, normalized to the vehicle control. A two-way ANOVA reveals a
1053 significant effect of time ($F_{3,32} = 5.949$, $p < 0.0024$) as well as treatment ($F_{3,32} = 10.13$, p
1054 < 0.0001). There is no significant interaction between time and treatment ($F_{9,32} = 1.765$, p
1055 $= 0.1145$). Post hoc comparisons between DMSO control and each treatment means were
1056 conducted using Dunnett's multiple comparisons. Ratio was significantly lower at all three
1057 time points for cannflavin A, while cannflavin B was significant only at 72 hours. ANA-
1058 12 did not cause a significant effect. **(C)** Relative tumorsphere radius expansion over time,
1059 showing significant inhibition of invasion upon cannflavin treatment. A two-way ANOVA
1060 reveals a significant effect of time ($F_{3,32} = 46.18$, $p < 0.0001$) as well as treatment ($F_{3,32} =$
1061 40.07, $p < 0.0001$). Notably, there is a significant interaction between time and treatment
1062 ($F_{9,32} = 8.749$, $p < 0.0001$), reflecting an earlier effect with cannflavin A, followed by
1063 cannflavin B, and finally ANA-12. Post hoc comparisons between DMSO control and each
1064 treatment means were conducted using Dunnett's multiple comparisons. Data represent
1065 mean ± SEM ($n = 3$; * $p < 0.05$; ** $p < 0.01$; *** $p < 0.001$; **** $p < 0.0001$; n.s., not
1066 significant).

1067 **FIGURE 6**

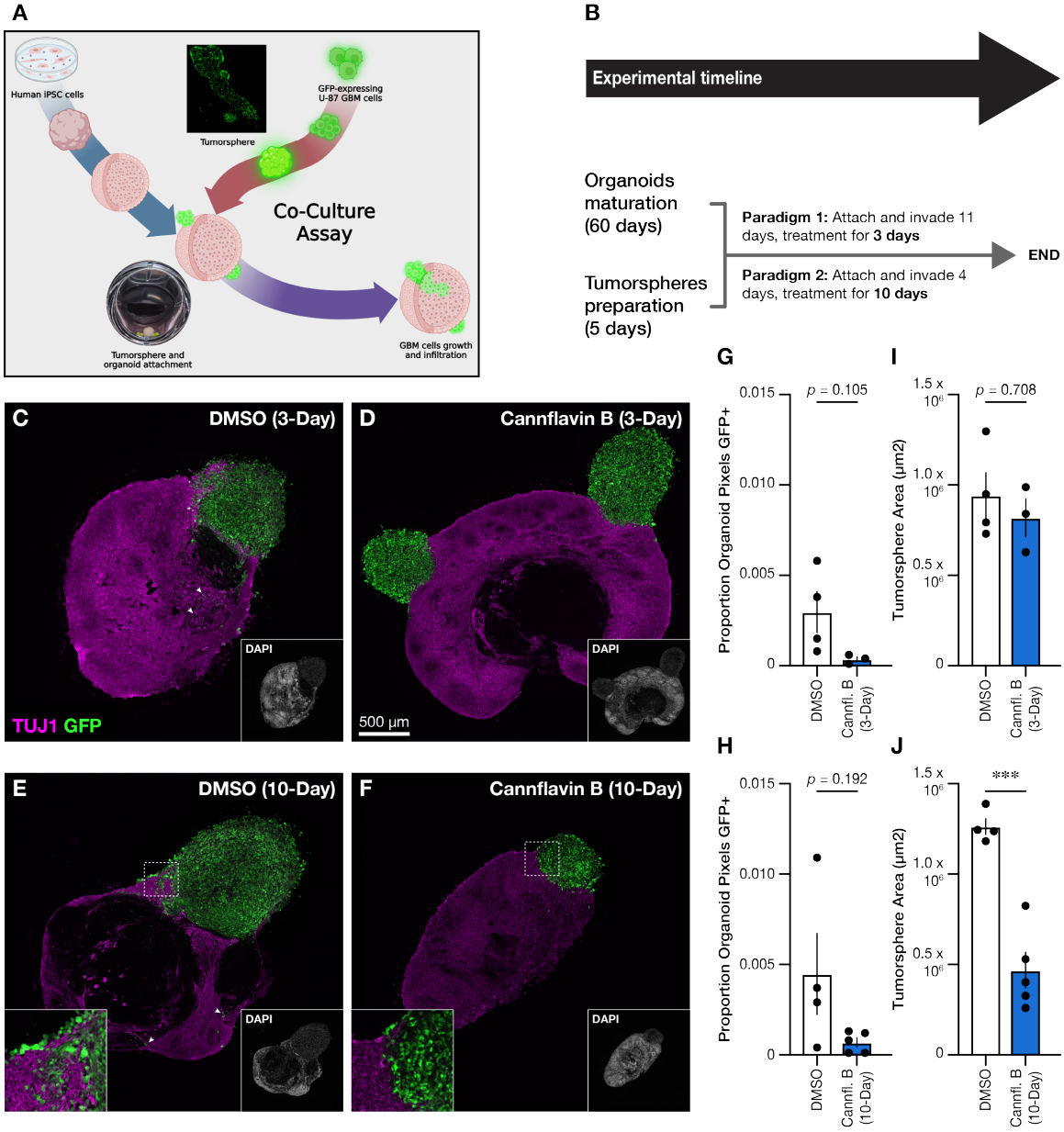

1068

1069 **Figure 6.** Cannflavin B reduces the size of attached tumorspheres to a cerebral organoid.

1070 **(A)** Schematic representation of cerebral organoid and U-87 tumorspheres co-culture

1071 model. Cerebral organoids matured for 60 days before introducing tumorspheres prepared

1072 with U-87 cells expressing GFP. **(B)** Two experimental timelines were tested: 11 days of

1073 co-culture followed by 3 days of applying cannflavin B to the culture media (final

concentration of 5 μM), and 4 days of co-culture followed by 10 days of applying cannflavin B (final concentration of 5 μM). **(C-F)** Representative capture of organoid with attached tumorsphere(s) for all conditions. **(G-H)** Proportion of GFP-positive pixels corresponding to U-87 cells within the cerebral organoid section area for the 3-day **(G)** and 10-day **(H)** conditions. **(I-J)** Estimation of tumorsphere size in the 3-day **(I)** and 10-day **(J)** conditions. The average tumorsphere area (GFP-positive cells, green) was significantly smaller after 10 days of cannflavin B treatment than in the corresponding DMSO control. Data represent mean ± SEM, with statistical significance determined by an unpaired two-tailed *t*-test (*** $p < 0.001$).

1083 **FIGURE 7**

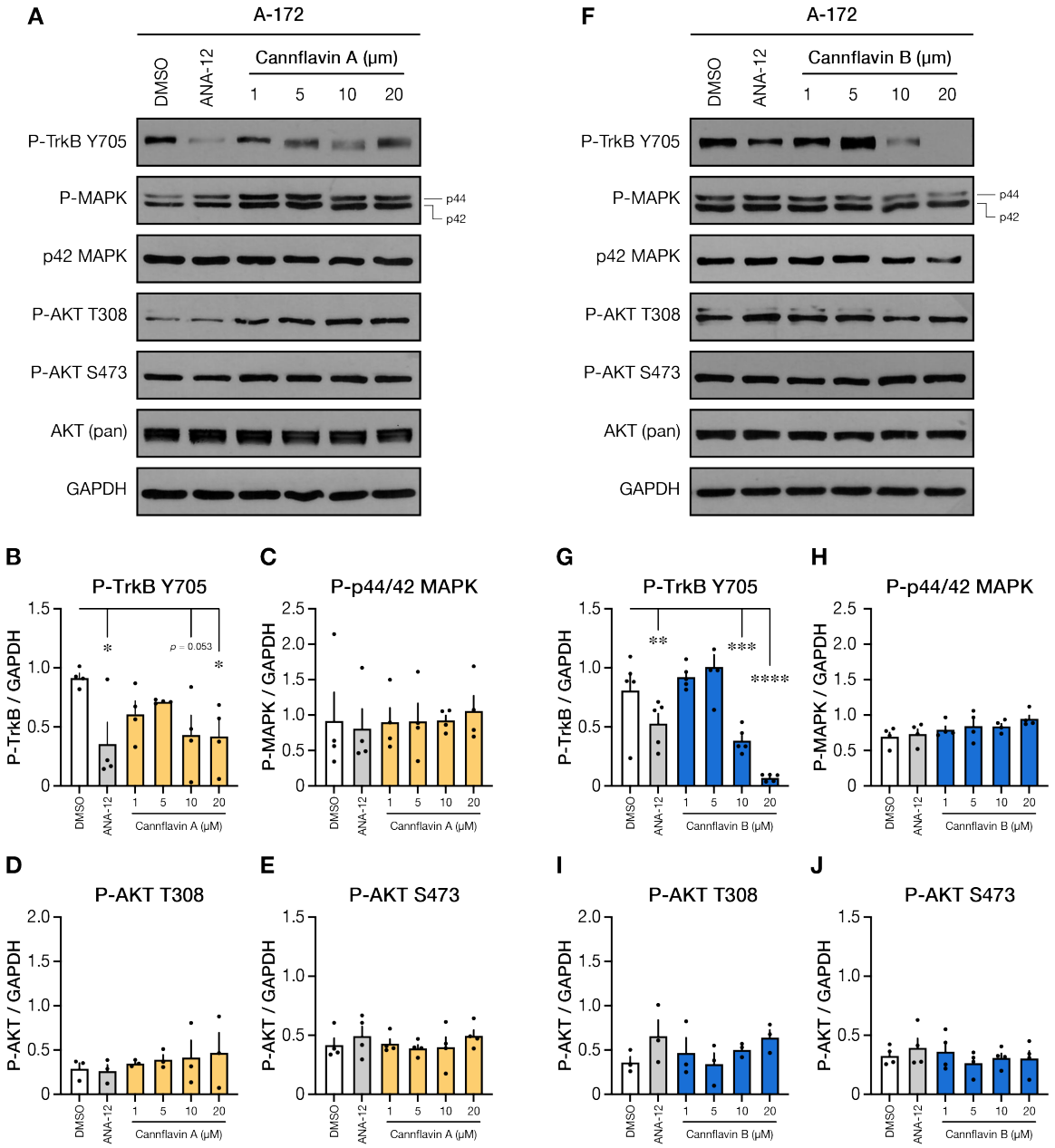

1084

1085 **Figure 7.** Cannflavin A and cannflavin B affect TrkB Y705 activation site but not
1086 downstream signaling in A-172 cells. Western blot analysis from A-172 cells treated for 6
1087 hours with cannflavin A **(A-E)** and cannflavin B **(F-J)** at various concentrations.
1088 Corresponding densitometry quantifications reveal a significant reduction in P-TrkB Y705
1089 signal, but not in P-MAPK and P-AKT. GAPDH (glyceraldehyde-3-phosphate

1090 dehydrogenase) was used as a loading control. Graphs show the mean ± SEM (n = 4) of
1091 the target/GAPDH ratio for cells treated as in **(A)** and **(F)**. Post hoc comparisons between
1092 DMSO control and each treatment means were conducted using Dunnett's multiple
1093 comparisons (* $p < 0.05$; ** $p < 0.01$; *** $p < 0.001$; **** $p < 0.0001$).

1094 **FIGURE 8**

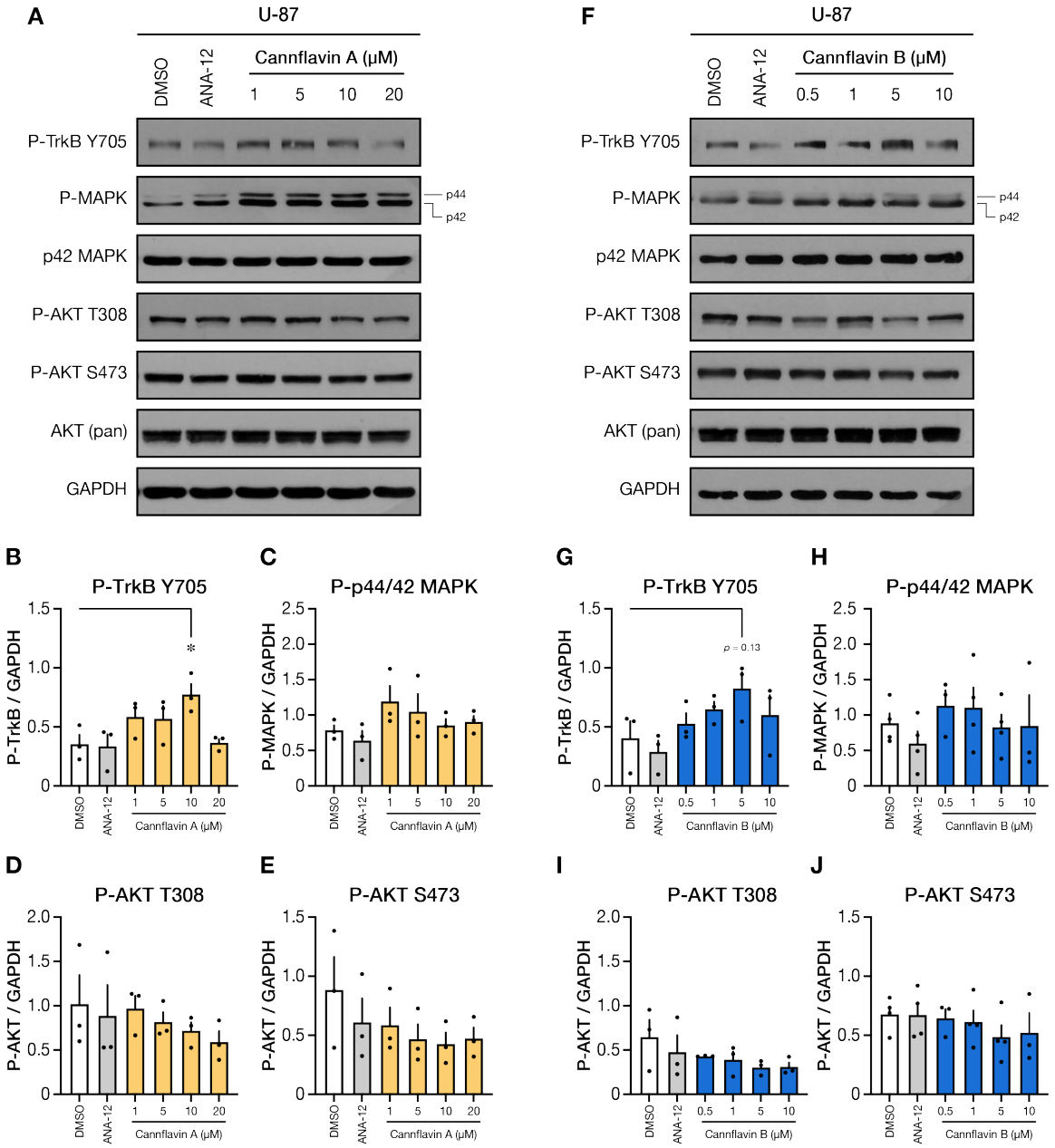

1095

1096 **Figure 8.** Cannflavin A and cannflavin B slightly increase TrkB Y705 activation site but
1097 not change downstream signaling in U-87 cells. Western blot analysis from U-87 cells
1098 treated for 6 hours with cannflavin A **(A-E)** and cannflavin B **(F-J)** at various
1099 concentrations. Corresponding densitometry quantifications reveal a significant reduction
1100 in P-TrkB Y705 signal, but not in P-MAPK and P-AKT. GAPDH (glyceraldehyde-3-

1101 phosphate dehydrogenase) was used as a loading control. Graphs show the mean ± SEM
1102 (n = 3) of the target/GAPDH ratio for cells treated as in **(A)** and **(F)**. Post hoc comparisons
1103 between DMSO control and each treatment means were conducted using Dunnett's
1104 multiple comparisons (* $p < 0.05$).

Supplementary Information for

Preclinical Study of Cannflavins A and B Action Against Glioblastoma Cells

Jennifer Holborn [a], Hannah Robeson [a,1], Ellis Chartley [a,1], Tiana Gluscevic [a,b,1], Adina Borenstein [a], Colby Perrin [a], Begüm Alural [a], Himain Perera [a], Tariq A. Akhtar [a], Nina Jones [a], Jasmin Lalonde [a,*]

* Correspondence to: jlalon07@uoguelph.ca

This PDF file includes:

Fig. S1 Cannflavin family members.

Fig. S2 LDH assay and TUNEL assay.

Fig. S3 Chrysoeriol and techtochrysin survival assay.

Fig. S4 Level of phospho-TrkB Y705 between A-172 and U-87 untreated cells.

Fig. S5 Graphical abstract.

Supplementary Table. Estimated IC50 for anti-survival effects of cannflavins and ANA-12.

Supplementary Video. Scratch migration assay video.

SUPPLEMENTARY FIGURE 1

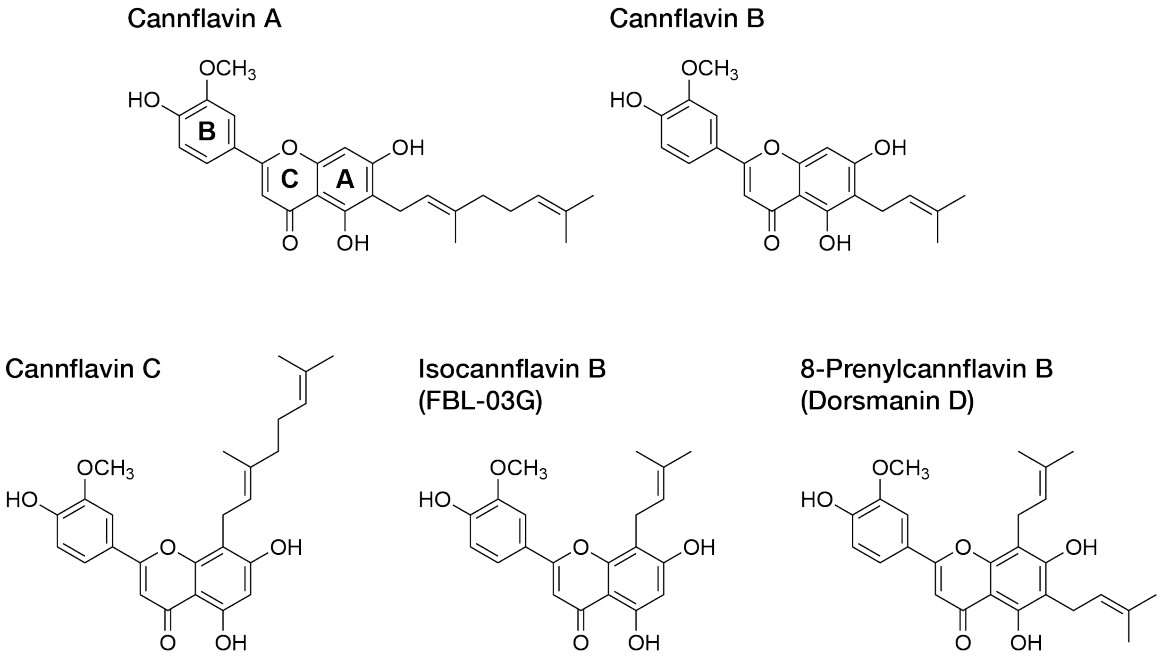

Supplementary Figure 1. Members of the cannflavin family. Position of each ring is labeled for cannflavin A.

SUPPLEMENTARY FIGURE 2

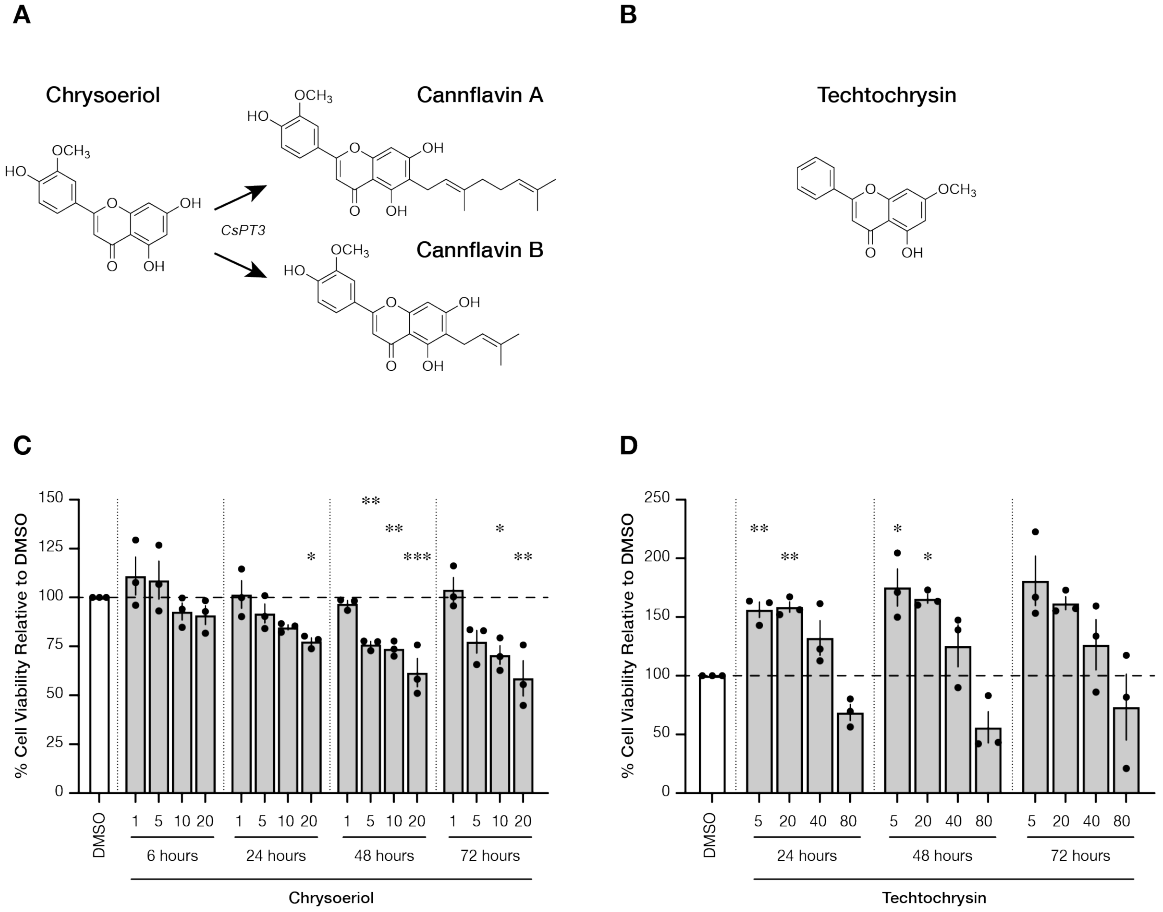

Supplementary Figure 2. Effect of chrysoeriol and techtochrysin on U-87 GBM cell survival. **(A)** Chemical structure of chrysoeriol and **(B)** techtochrysin. As proposed by Real and colleagues (2019), *C. sativa* prenyltransferase 3 (CsPT3) catalyzes the biosynthesis of cannflavins from chrysoeriol. **(C-D)** U-87 cells were treated with increased concentrations of chrysoeriol (1-20 μM) or techtochrysin (5-80 μM), and cell viability was measured at the indicated time-points using the resazurin reduction assay. DMSO was used as a vehicle control. Application of chrysoeriol, but not techtochrysin, reduced the viability of U-87 GBM cells in a dose- and time-dependent manner. A one-way ANOVA was used to analyze the data from each cell line, treatment, and time independently with DMSO as the reference control. Tukey's honestly significant

difference (HSD) post hoc test: * $p < 0.05$, ** $p < 0.01$, *** $p < 0.001$. Graphs represent mean ± SEM ($n = 3$).

SUPPLEMENTARY FIGURE 3

A A-172 LDH Release Assay (24 h)

	% LDH release	SEM
Lysis buffer		
Positive control	100	–
Vehicle (DMSO)		
Negative control	1.77	0.65
Cannflavin A		
10 μM	3.57	0.84
20 μM	2.54	0.66
Cannflavin B		
10 μM	4.43	1.43
20 μM	5.38	1.44
ANA-12		
10 μM	2.01	0.48
50 μM	11.35	3.63

B U-87 LDH Release Assay (24 h)

	% LDH release	SEM
Lysis buffer		
Positive control	100	–
Vehicle (DMSO)		
Negative control	1.57	0.29
Cannflavin A		
10 μM	0.96	0.09
20 μM	1.03	0.08
Cannflavin B		
10 μM	0.81	0.05
20 μM	0.88	0.07
ANA-12		
10 μM	1.61	0.26
50 μM	10.71	0.64

C

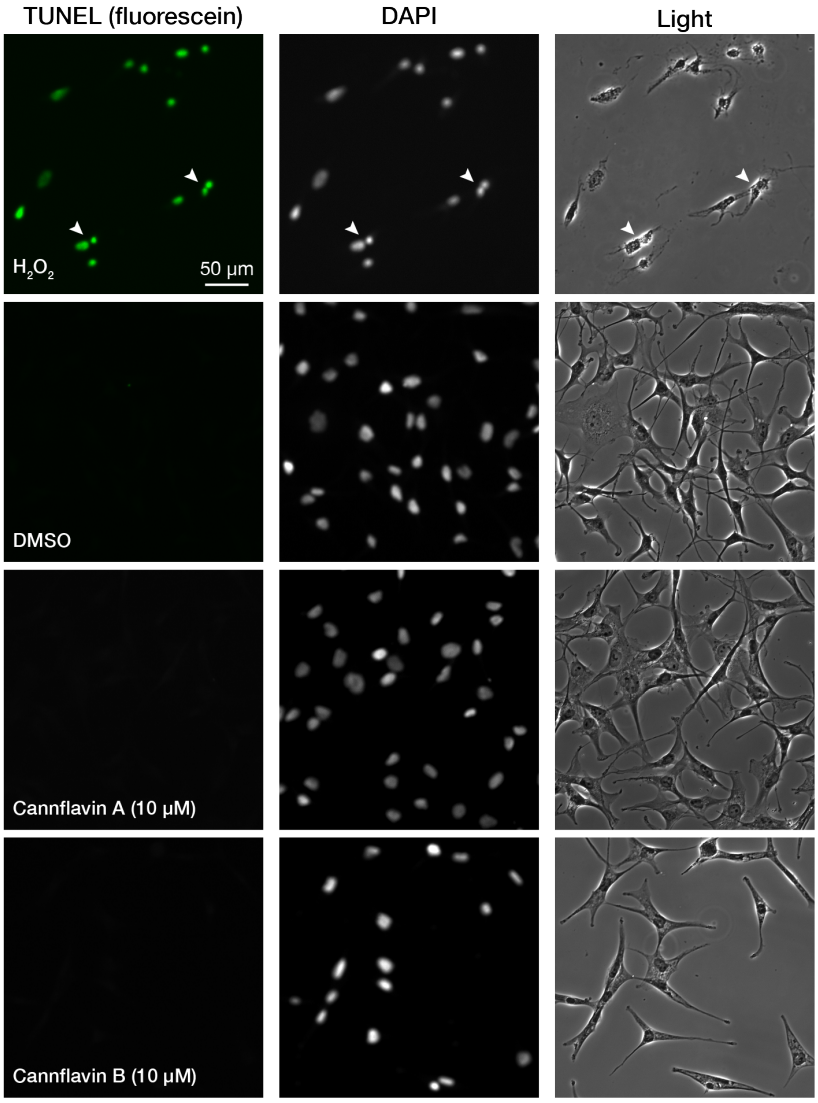

Supplementary Figure 3. Effects of cannflavins A and B on LDH release and DNA fragmentation. **(A)** A-172 and **(B)** U-87 GBM cells were treated with cannflavin A or cannflavin B at 10 and 20 μM final concentrations, or ANA-12 (10 and 50 μM final concentration), and percent LDH release into cell culture media was quantified using the Invitrogen CyQUANT LDH Cytotoxicity Assay Kit. **(C)** Representative immunofluorescent images of A-172 GBM cells after 24 hours of treatment with cannflavins (10 μM final concentration) probed using TUNEL (fluorescein, green signal represent the occurrence of double-stranded DNA breaks). Nuclei were stained with DAPI (middle panels). Hydrogen peroxide (H_2O_2) was used as a positive control (applied directly to cell culture media for 10 minutes at a final concentration of 100 μM), and DMSO as the vehicle control for cannflavins. Arrowheads in the positive control condition show fragmented nuclei indicative of apoptosis. Scale bar = 50 μm.

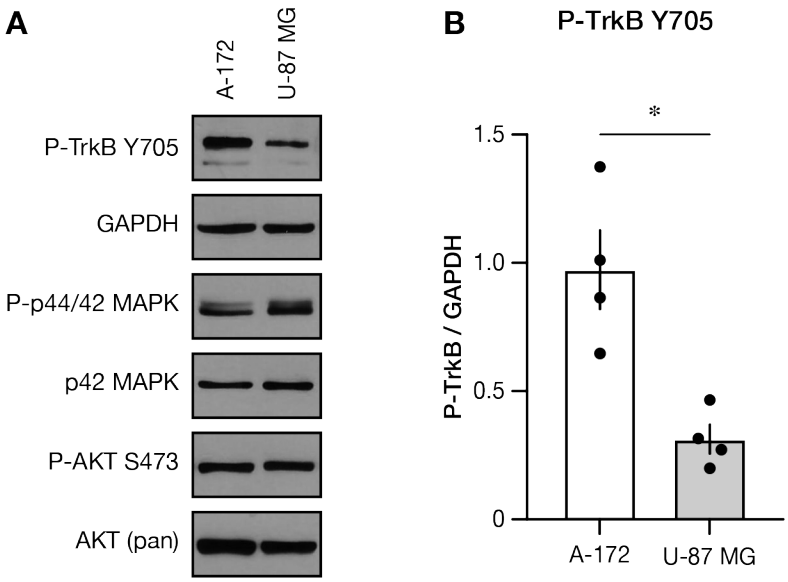

Supplementary Figure 4. Level of phospho-TrkB Y705 between A-172 and U-87 untreated cells. **(A)** Representative western blots for phospho-TrkB Y705 and downstream signaling effectors. **(B)** Densitometry quantification shows a significantly higher abundance of phospho-TrkB Y705 in A-172 cells than in U-87 cells. * $p < 0.05$, two-tailed unpaired t-test. Graph represents mean ± SEM ($n = 4$).

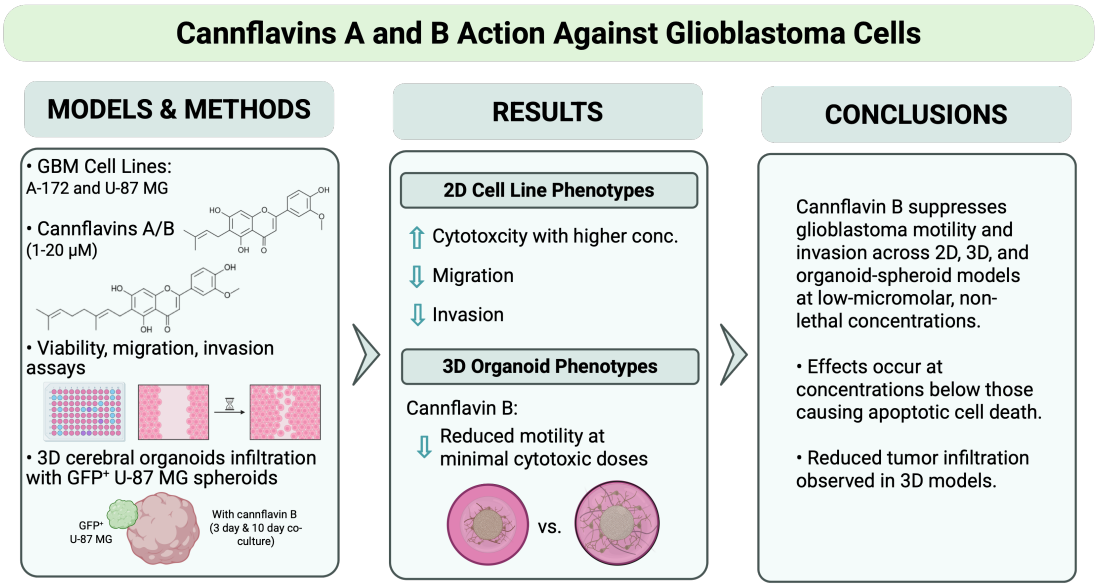

Supplementary Figure 5. Graphical abstract.

SUPPLEMENTARY TABLE

A-172		U-87 MG	
Condition	**IC_{50} (µM)**	**Condition**	**IC_{50} (µM)**
Cannflavin A (6 h)	>200	Cannflavin A (6 h)	>200
Cannflavin A (24 h)	173.4	Cannflavin A (24 h)	>200
Cannflavin A (48 h)	88.5	Cannflavin A (48 h)	187.9
Cannflavin B (6 h)	76.1	Cannflavin B (6 h)	63.9
Cannflavin B (24 h)	10.2	Cannflavin B (24 h)	20.2
Cannflavin B (48 h)	4.2	Cannflavin B (48 h)	25.1
ANA-12 (6 h)	168.8	ANA-12 (6 h)	156.2
ANA-12 (24 h)	39	ANA-12 (24 h)	48.0
ANA-12 (48 h)	27.9	ANA-12 (48 h)	49.2

Supplementary Table. The estimated IC_{50} for the survival assay is shown in Figure 1.

SUPPLEMENTARY VIDEO

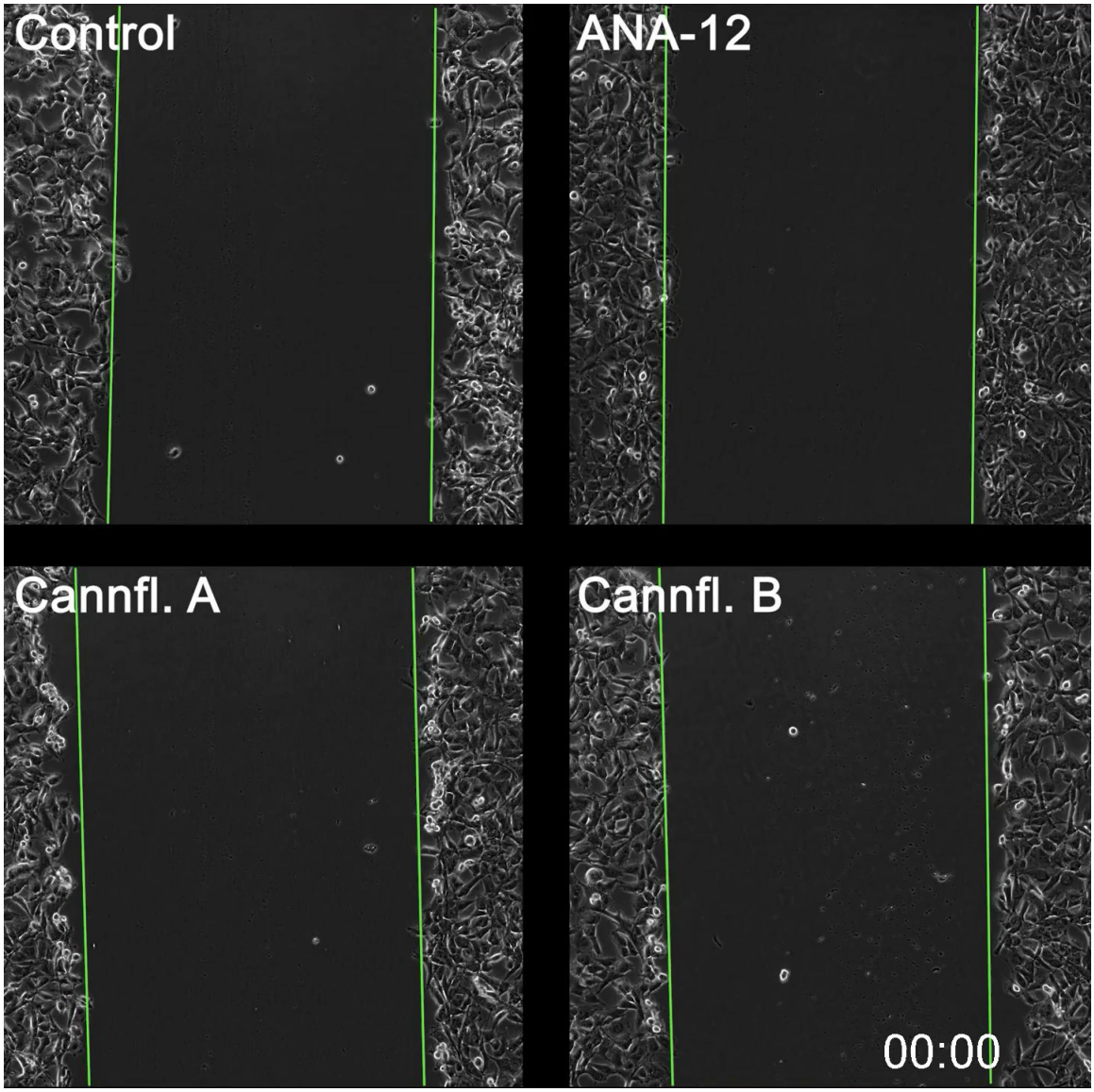

Supplementary Video. Scratch migration assay video. The green lines represent the initial boundaries ($t = 0$) of the scratched wound.